Physics – Uspekhi **60** (1) 91 – 107 (2017) ©2017 Uspekhi Fizicheskikh Nauk, Russian Academy of Sciences

INSTRUMENTS AND METHODS OF INVESTIGATION PACS numbers: 52.55.Fa, 82.80.Ms, 82.80.Rt

Application of dynamic mass spectrometers for investigations in the field of thermonuclear synthesis

N N Aruev

DOI: https://doi.org/10.3367/UFNe.2016.05.037807

Contents

Abstract. This review discusses the design, analytical characteristics, and some applications of two types of dynamic mass spectrometers that have been developed at the Ioffe Institute, Russian Academy of Sciences: the magnetic resonance mass spectrometer (MRMS) and time-of-flight mass spectrometer (TOFMS), the latter of which the inventors named the mass reflectron. With the aid of an MRMS, it was possible to measure the half-life of tritium, which is a fusion fuel candidate, and to start investigating how deuterium plasma interacts with the structural materials of the spherical tokamak Globus-M. The research done shows that mass reflectrons can be used successfully in the analysis of tritium-containing fusion fuel gas mixtures.

Keywords: dynamic mass spectrometers, magnetic resonance mass spectrometers, time-of-flight mass spectrometers, resolution, sensitivity, dynamic range, fuel gas mixtures, hydrogen and helium isotopes, analysis of tritium-containing mixtures, tritium half-life

1. Introduction

Dynamic mass spectrometers are devices in which the acceleration, motion, and mass separation of analyzed ions are carried out by pulsed or radiofrequency electric fields. Altogether, there are about 10 types of dynamic mass analyzers in the world, and two of them — magnetic resonance and time-of-flight mass spectrometers — were developed, were manufactured, were investigated in detail, and found wide applications in the mass spectrometry laboratory at the Ioffe Physical-Technical Institute, RAS (PTI).

Late in the 1970s – early 1980s, several very important scientific issues appeared that attracted the attention of physicists. They include the determination of the mass of an electron antineutrino [1–3] and the related measurement of the mass difference of the $^3T^+ - {}^3He^+$ doublet [4, 5]; the vigorous development of plasma physics; the construction of thermonuclear facilities in many places, mainly toroidal and, later, spherical tokamaks; the related search for methods to analyze fuel gas mixtures containing hydrogen and helium isotopes, in particular, tritium [6, 7]; and studies of the interaction of hydrogen and helium isotopes with construction materials used in thermonuclear facilities [8, 9]. At about this time, the tritium half-life was measured in the USA by the absolute counting method to be $T_{1/2} = 12.43 \pm 0.05$ year, which exceeded the value accepted in the Soviet Union by 0.08 year, i.e., by four weeks. All these issues were directly related to mass spectrometry and chemical and isotope analysis of materials. Because the mass spectrometry laboratory at the PTI had a large enough stock of operating instruments and we had some experience in working with tritium and in precision measurements of fundamental physical constants [11], we decided to participate in these studies and have continued our investigations.

2. Magnetic resonance mass spectrometers

The development of magnetic resonance mass spectrometers (MRMSs) was started at the Leningrad Physical-Technical Institute in the early 1950s, and they continue to be upgraded.

N N Aruev Ioffe Institute, Russian Academy of Sciences,
ul. Politekhnicheskaya 26, 194021 St. Petersburg, Russian Federation
E-mail: aruev.mass@mail.ioffe.ru

Received 7 December 2015
Uspekhi Fizicheskikh Nauk **187** (1) 99 – 117 (2017)
DOI: https://doi.org/10.3367/UFNr.2016.05.037807
Translated by M N Sapozhnikov

For more than 50 years, work on the development and application of these instruments was performed by B A Mamyrin (25.05.1919– 05.03.2006) and his pupils and colleagues. Altogether, seven mass spectrometers were built, with five of them still in existence (all at the PTI) but only one bing actively used.

The operation principle of MRMSs is based on the dependence of the circular frequency of ions moving over a circular orbit in a permanent homogeneous magnetic field on the field strength and the ion mass-charge ratio. The cyclotron frequency ω_c of ions with charge Zq and mass M in a homogeneous permanent magnetic field H is defined by the expression

$$\omega_c = \frac{ZqH}{cM}\,, \tag{1}$$

where c is the speed of light. The magnetic field provides a perfect temporal and spatial focusing of ions. The period of revolution of ions over a circular orbit is independent of their energy and angle of departure from a source and is defined by the expression

$$T_c = \frac{2\pi Mc}{ZqH}\,, \tag{2}$$

or for single-charged ions,

$$T_c \approx 652\frac{M}{H}\,, \tag{3}$$

where T_c is measured in microseconds, M in atomic mass units (a.m.u.), and H in oersteds. Thus, the expression for the radius of motion ρ of a charged particle with the mass–charge ratio M/q in a permanent magnetic field H under the action of the electric potential U,

$$\rho = \frac{(2UM/q)^{1/2}}{H}\,, \tag{4}$$

gives the relation between ρ and the accelerating voltage in the ion source. Rough calculations are usually performed with the help of the expression $\rho = 144(UM/q)^{1/2}/H$, where ρ is measured in centimeters, the accelerating voltage U in volts, the ion mass M in a.m.u., the ion charge in elementary charges, and the magnetic field in oersteds.

The authors of [12] were probably the first to propose that atomic masses be determined by measuring the time of flight of ions in a magnetic field along a circular path, but this work did not become well known. About ten years after the end of the Second World War, the rapid development of mass spectrometry started as one of the most accurate techniques for studying the composition of matter, and three research groups in the USSR and USA [13–15] proposed almost simultaneously independent methods for determining atomic masses by measuring cyclotron periods. Study [14] by fourth-year student V B Fiks of the Physico-Mechanical Department at the Leningrad Polytechnic Institute was continued in one of the laboratories at the PTI where isotope separation was studied within the framework of the Atomic project. It is probably not worth considering here in detail the design of magnetic time-of-flight mass spectrometers, including two American instruments, but we would like to describe briefly the main stages of the development of MRMSs.

The first work performed at the PTI [16] contained three schemes of time-of-flight magnetic mass spectrometers which were successively built and investigated. The spectrometers were constantly upgraded and became more involved. The operation principle of the third model of the instrument for measuring atomic masses by the cyclotron frequency can be described as follows.

Ions produced in the ion source travel a half turn in a permanent magnetic field and enter a three-grid modulator. The outer grids of the modulator are grounded, and voltage pulses with duration Δt and repetition rate ω are applied across the middle grid. The ions passing through the modulator are accelerated and the radius ρ increases. The ions bend round the source and again enter the modulator. If the pulse repetition rate ω is proportional to the cyclotron frequency of ions ω_c, i.e. $\omega = n\omega_c$, where n is an integer or the number of the modulation voltage harmonic, then ions can perform several revolutions along the helical trajectory in the magnetic field, reach the collector, and be detected. During this motion, the ions are separated by their masses according to the time of flight, i.e., the cyclotron period. Light ions enter the collector first, while the heaviest ions enter last.

The authors of [16] showed that the usual expression for the resolving power $R = M/\Delta M$, where M_1 and M_2 are the masses of ions of two kinds, $M = (M_1 + M_2)/2 \approx M_1 \approx M_2$, $\Delta M = M_2 - M_1$, is transformed into the expression

$$R = \frac{M}{\Delta M} = \frac{\omega}{\Delta\omega}\,, \tag{5}$$

where $\Delta\omega$ is the mass peak width at a certain height. The resolving power at the half-maximum of the mass line for the $^{85}Rb^+ - {}^{87}Rb^+$ doublet with $n = 3$ was measured to be ≈ 1200 [16]. The study of the operation of this mass spectrometer led to important conclusions: (i) the use of the higher harmonics of the modulation voltage ($n \gg 1$) provides a considerable increase in the output current of the mass spectrometer, thereby increasing its sensitivity, and (ii) measurements of ion masses are reduced to frequency measurements.

From the very beginning, the aim of studying the systems of resonance mass spectrometers at the PTI was to build an analytic instrument with a high resolving power and high sensitivity for solving a number of gas-dynamic problems. The first operating instrument [17] was built using the setup [16] described above. Therefore, here we consider only the factors affecting the analytic characteristics of mass spectrometers. The sensitivity of pulsed mass spectrometers drastically decreases as opposed to that of magnetic static mass spectrometers, because the detector current exists only for short time intervals and is absent in time intervals between pulses. The aperture ratio and sensitivity of a pulsed MRMS also decrease during the propagation of ion packets through three modulator grids.

The greater the number of revolutions performed by the ion packet in the drift orbit ($n = 1-5$), the higher the resolving power and the lower the aperture ratio and sensitivity of the instrument.

Because the resolving power of the MRMS is determined by the ion packet duration, i.e., by the size of packets in the direction of their motion, slits up to a few millimeters in width can be used in the ion source and all diaphragms, thereby considerably increasing the operation current and sensitivity of the mass spectrometer without a noticeable decrease in the resolving power. Note that, to obtain $R \sim (5-10) \times 10^3$ in static magnetic mass spectrometers, slit widths of only a few dozen micrometers are used, i.e., several hundred times narrower than in resonance mass spectrometers.

To increase the coefficient of usage of the source current and the sensitivity of a pulsed MRMS, ions were accumulated in the ionization chamber during the time between ejecting pulses, which were synchronized via a delay line with pulses delivered to the modulator. As a result, the ion current from the source became pulsed, but the current density in the pulse increased T/τ_1 times, where T is the repetition period of voltage pulses applied to the source and modulator and τ_1 is the ion packet duration mainly determined by the width of the ionization chamber of the source [17].

The constructed pulsed MRMS had the following analytic characteristics. With a resolving power of 4–5 thousand at the half-maximum of the mass line, the output ion current was $\approx 10^{-11}$ A. One of the advantages of the instrument in the opinion of the authors of [17] was the good shape of the mass spectrum line and the absence of 'tails' in the peak pedestal. The main disadvantages of this mass spectrometer were: (i) the necessity of working with a large number of ion revolutions in the drift orbit ($n = 3-5$) for obtaining a high resolving power, which reduced the output current and sensitivity of the instrument; (ii) the pulsed operation mode of the source; and (iii) the presence of harmonics, i.e., the possibility of obtaining peaks of the same mass for different repetition rates of pulses applied to the modulator and ion source.

To eliminate these disadvantages, a new design of a pulsed MRMS was proposed at the PTI [18], in which a trapezoid periodic voltage is applied to the modulator, while the ion source operates in the continuous mode. The study of this instrument allowed the authors to explain theoretically the presence of three different MRMS operation regimes: compensation and resonance regimes, and the direct throwing regime in which ions acquire the velocity and radius increments after the first passage thorough the modulators that are sufficient for entering the exit slit of the instrument. It was also shown that the high resolving power (on the order of a few thousand) can be obtained for one revolution of ions in the drift orbit, i.e., only for two accelerations of ions in the modulator.

In the compensation operation regime of the MRMS, ions that acquire lower energy in the first acceleration in the modulator acquire higher energy during the second acceleration, and, *vice versa*, ions that first acquire higher energy receive lower energy during the second acceleration. Thus, after two accelerations, the energy scatter for a certain part of the ions will be compensated and the energy of all the ions in the packet will be the same. The continuous variation in frequency in a small range does not violate the compensation of the energy of ions in the packet, and the ion packet entering the exit slit of the mass analyzer produces a compensation peak of the ion current. Two compensation peaks located on both sides of the resonance peak correspond to each harmonic of the modulating voltage. The resonance peak amplitude is approximately half the compensation peak amplitude, and its amplitude is noncritical to frequency variations in a quite broad frequency range, unlike the amplitude, of compensation peaks. It was later found that the theory developed for the trapezoid modulating voltage [18] is also valid for the sinusoidal voltage [19].

A very important result, which completely determined the direction of development of magnetic resonance instruments, was obtained somewhat earlier [20] in the study of the acceleration of ions in a two-gap symmetric modulator. The grounded side electrodes of this modulator are located at a distance a from the middle electrode to which the high-frequency sinusoidal voltage $U_m \sin(\omega t)$ is applied. If ions enter the modulator with velocity v_0, they receive under the action of the modulating voltage the velocity increment Δv, which in the first approximation sinusoidally depends on the ion entry time into the modulator.

This increment Δv can be considered a function of the phase φ of the modulating voltage which corresponds to the moment ions pass through the middle grid of the modulator. In this case,

$$\Delta v = U_m \cos\varphi \, \frac{1-\cos\theta}{\theta} , \tag{6}$$

$$\theta = \frac{a\omega}{v_0} , \tag{7}$$

where U_m and ω are the modulation voltage amplitude and frequency, respectively, and a is the distance between modulator grids. It is shown in [19] that the factor $(1-\cos\theta)/\theta$ has a maximum at the phase angle

$$\theta \approx \frac{3\pi}{4} . \tag{8}$$

This means that ions will receive the maximum velocity and radius of motion increments if a and ω in (7) are selected so that the phase angle of the high-frequency modulating voltage changes during the flight by $3\pi/4$.

Equations (6) and (7) relate geometrical, electric, frequency, and phase parameters of resonance instruments and are used to calculate their analytic characteristics. Condition (8) proved to be also valid for a two-gap symmetric slit modulator; however, in this case, a is not the distance between the central and side electrodes of the modulator but an effective quantity taking into account the sag of electric fields in the slit of the electrodes.

The instrument in [21] built based on these concepts had a resolving power on the order of 10–12 thousand at the half-maximum of the mass line and high sensitivity in the compensation regime and was used to measure mass spectra of residual gasses in the chamber of the MRMS analyzer in the mass range from 2 to 45 a.m.u.

The second mass spectrometer [22] was constructed especially for measuring one of the most important fundamental physical constants — the proton magnetic moment in nuclear magnetons. Therefore, to improve the measurement accuracy, it was necessary to obtain the maximum possible resolving power in the resonance regime in which the resonance frequency of ions is virtually independent of the modulating voltage amplitude and which allows accurately calculating the modulator correction related to the acceleration of ions in modulator gaps, i.e., to the perturbed cyclotron frequency.

By definition, the proton magnetic moment μ_p/μ_n in nuclear magnetons is described by the expression

$$\frac{\mu_p}{\mu_n} = \frac{\omega_n}{\omega_{c,p}} , \tag{9}$$

where ω_n is the proton spin precession frequency (nuclear magnetic resonance frequency) and $\omega_{c,p}$ is the proton cyclotron frequency measured in the same magnetic field. Because ion cyclotron frequencies $\omega_{c,i}$ ($^4He^+$, $^{20}Ne^{++}$, $^{20}Ne^+$) rather than proton frequencies were measured in experiments, the frequency $\omega_{c,p}$ was calculated from the equality

$$\omega_{c,p} M_p = \omega_{c,i} M_i . \tag{10}$$

To take into account the influence of parasitic electric fields on ion cyclotron frequencies, the linear extrapolation of $\omega_{c,i}$ for pairs of ions with masses M_1 and M_2 (for example, $^4He^+$, $^{20}Ne^{++}$) to the zero mass was performed. This procedure corresponds to the measurement of the cyclotron frequency of an ion accelerated by infinite voltage compared to which the influence of parasitic electric fields is negligible. However, the necessary condition for the extrapolation is the equality or stability of parasitic fields along the trajectory of motion of ion pairs, which is extremely difficult to fulfill.

Nevertheless, the high resolving power of the MRMS (30–35 thousand at the peak half-maximum), the use of the method combining the cyclotron signal with the nuclear magnetic resonance signal, and careful account for possible measurement errors provided the measurement of μ_p/μ_n with a relative error of ≈ 7.3 ppm (parts per million) [22, 23].

To eliminate a possible error during the extrapolation of $\omega_{c,i}$ to the zero mass, a two-section ion source was developed from which ions of two masses simultaneously escaped in pairs $^4He^+ - {}^{20}Ne^{++}$, $^4He^+ - {}^{20}Ne^+$, $^4He^+ - {}^{40}Ar^{++}$, and $^4He^+ - {}^{40}Ar^+$ [11, 24]. As a result, the influence of parasitic electric fields on the cyclotron frequencies of ions in pairs was considerably weaker than in [20, 22]. In addition, the inhomogeniety of the magnetic field in the working orbit was considerable reduced to $\Delta B_z/B_0 \approx 7 \times 10^{-6}$ (here, B_0 is the magnetic field at the center of the magnet gap). In [11, 24], all three magnetic field components were measured in a working orbit 224 mm in diameter: the vertical, ΔB_z, radial ΔB_ρ, and azimuthal, ΔB_φ [25]. The resolving power at the half-maximum of the mass line in the entire range of ion masses measured (4–40) was $\approx 5 \times 10^4$.

The instrument operated in the resonance regime [18]. This allowed the authors to calculate accurately the modulator correction related to the fact that ions in the modulator are accelerated and the velocity increment is not exactly sinusoidal. Also, corrections were introduced caused by the magnetic properties of the MRMS analyzer chamber, the magnetic action of the cathode filament current in the ion source, and the relativistic correction, and all possible measurement and calculation errors were estimated. As a result, the value $\mu_p/\mu_n = 2.7927744 \pm 0.0000012$ $(\pm 0.43 \times 10^{-6})$ was obtained, which entered, without changes, into the concordance of fundamental physical constants in 1973 [26] and determined the values of a number of electromagnetic physical constants until the next concordance in 1986 [27].

Studies [18, 19, 21–23] concluded the first stage in the development of magnetic resonance mass spectrometers, showed methods for calculating the analytic characteristics of MRMSs and outlined two ways for the further development of these instruments: the achievement of the maximum possible resolving power for measuring fundamental physical constants, atomic masses, and mass differences, and the achievement of the maximum absolute and isotopic sensitivity, in particular, for studying the isotopy of noble gases in natural and technogenic samples. Because all the later studies on the updating and modernization of MRMSs concerned the development of the theory and improvement of the operation of individual units or their parameters and systems of these instruments, rather than the operation principle of the mass spectrometer as a whole, it seems pertinent to present here the MRMS schematic (Fig. 1) and describe its operation principle.

The analyzer is located in a homogeneous magnetic field H. The ions of gasses under study are produced in a Nier source by electron impact, escape from it through a slit S_0, and move over a circular orbit. The preliminary separation of the ion beam is performed in the first static 180° stage of the instrument. Ions with close values of M/q enter the modulator and are subjected to the action of a high-frequency electric field in two gaps between three plane parallel electrodes with slits S_1. The outer electrodes of the modulator are grounded and a sinusoidal voltage is applied to the central electrode with a frequency greatly exceeding (the harmonic number $n = 100-200$) the cyclotron frequency of ions in the given magnetic field. The ion beam passing through modulator gaps is modulated over energy and hence over the trajectory radius.

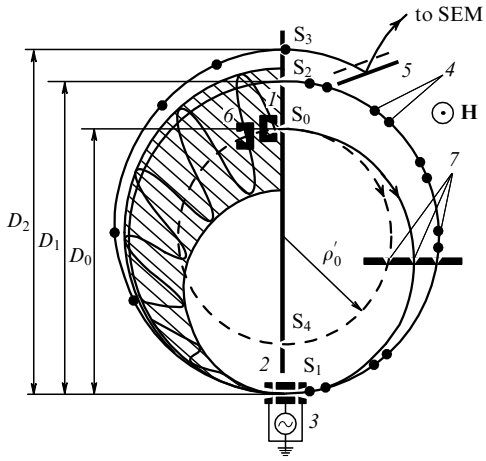

Figure 1. Schematic of a magnetic resonance mass spectrometer: (*1*) ion source, (*2*) modulator, (*3*) high-frequency generator, (*4*) ion packets cut out by the drift slit S_2 from a modulated beam, (*5*) ion reflector, (*6*) 360° ion collector, (*7*) aperture slits, S_0: exit slit of the source, S_1: slits in modulator electrodes, S_2: drift slit, S_3: exit slit of the analyzer, S_4: control slit, D_0, D_1, and D_2: diameters of orbits, SEM: Secondary Electron Multiplier.

The instant position of the ion beam is shown in the hatched region in Fig. 1. The drift slit S_2 cuts the short ion packets from the beam, which, after passing another half turn in the magnetic field, again enter the modulator. If the amplitude, frequency, and phase of the modulating voltage are set correctly, the ion packets receive the second energy and radius increments required for their entering the exit slit S_3. Using a reflecting gap or cylindrical capacitor, the beam is extracted from the magnetic field region and falls on the secondary electron multiplier (SEM-1 or SEM-6), whose current is detected with an electrometric amplifier.

As pointed out in the Introduction, the necessity for accurate measurements of the mass difference of tritium and helium-3 atoms (ions) appeared after the publication of papers [1—3] in which the upper boundary of the β spectrum of tritium was determined: the β decay of the tritium nucleus produces a helium-3 nucleus, an electron, and an electron antineutrino with an energy release of about 18.6 keV,

$$^3T \rightarrow {}^3He^+ + e^- + \tilde{\nu} + 18.6 \text{ keV}\,. \qquad (11)$$

This means that, if the mass difference between tritium and helium-3 atoms, the electron mass, and the final (maximum) energy of the β spectrum of tritium are accurately known, we can estimate the mass of an electron neutrino $\tilde{\nu}$. The mass difference $\Delta M = M(^3T) - M(^3He)$ measured with a mass

spectrometer in a.m.u. can be represented in energy units with the help of the corresponding recalculation coefficient. These measurements were complicated by extremely strict requirements. First, the mass difference is $\Delta M = M(^3\mathrm{T}) - M(^3\mathrm{He}) \approx 0.00002$ a.m.u. Therefore, the resolving power of the mass spectrometer by the mass line base should be $R = M/\Delta M = 3/0.00002 = 1.5 \times 10^5$. Second, because the mass of an electron antineutrino is vanishingly small, being close to zero, assuming ~ 1 eV (1 a.m.u. ≈ 930 MeV), the relative error of mass difference measurement should be about 10^{-9} a.m.u. Third, tritium is a radioactive substance and its admission into mass analyzers leads to an increase in the dark current of secondary electron multipliers of all types and microchannel planes by several orders of magnitude, which makes impossible accurate measurements of masses or mass differences.

The development of MRMSs with the resolving power $R = 1.5 \times 10^5$ by the peak base began with the formation of the theory of motion of ions in the instrument (see Fig. 1) in the compensation operation regime [28]. The motion of ions in the mass analyzer from the source to the detector can be separated into nine parts and described by nine transcendent equations connecting the phases and angles of flight of an ion in gaps between electrodes of the three-chamber modulator in the first and second flights. The geometrical, electric, and frequency parameters of the analyzer are contained in these equations as coefficients. By specifying the phase φ_{01} during the first flying of ions in the modulator and solving the system equations obtained, we find the increment of the diameter of the ion orbit after two passages of ions in the modulator and also the ion packet shape, size, and position in front of the exit slit S_3. In [28], analytic expressions were also obtained for the MRMS resolving power by the mass line base and for the analyzer sensitivity. All the optimal parameters of the analyzer were selected with the help of a special computer program to obtain the maximum sensitivity for the specified resolving power $R = 1.5 \times 10^5$.

Based on these calculations, an MRMS was constructed which was adjusted to the maximum resolving power by moving the drift slit S_2 in a small range and rotating the exit slit S_3 with respect to the magnetic line of forces and tuning all the supply voltages and currents. The results of calculations are in good agreement with experiments. The careful adjustment of all the parameters and $n = 110$ provided the resolving power of the mass spectrometer at the half-maximum of the mass line of $^3\mathrm{He}^+$ $R_{0.5h} = 350{,}000$, and the peak had a good shape typical for MRMSs.

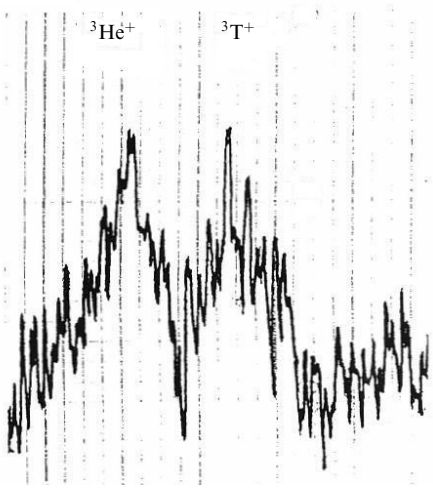

Figure 2. Mass spectrum of the $^3\mathrm{He}^+ - {}^3\mathrm{T}^+$ doublet. $\Delta M = 0.00002$ a.m.u.

To illustrate the resolving power of the instrument, a few series (a few dozen spectra) of the $^3\mathrm{T}^+ - {}^3\mathrm{He}^+$ doublet were recorded, one of which is presented in Fig. 2. It can be seen that the spectrum is covered by noise current pulses caused by the β decay of tritium nuclei on the surface of multiplier dynodes and surrounding elements in the MRMS detection system. The constant component of the noise current is 2–3 orders of magnitude greater than the amplitude of double peaks. Despite the presence of the background β electron current, the $^3\mathrm{T}^+$ and $^3\mathrm{He}^+$ peaks are well enough resolved, giving the estimate of the mass difference $\Delta M = M(^3\mathrm{T}) - M(^3\mathrm{He}) \approx 18{,}600$ eV. However, the measurement error was so large (≈ 200 eV) that this result was not published at that time.

3. Ion beam detector

The appearance of the background current after the admission of gaseous tritium to an MRMS analyzer was unexpected and unclear, because no data on mass spectrometric measurements were reported in the literature in the late 1970s. Studies of the background current caused by the β decay of tritium showed that this current increased upon increasing the partial pressure of tritium in the mass analyzer. The current was proportional to the area of first dynodes when secondary electron multipliers SEM-1 or SEM-2 were used in the detector or to the area of the entrance window when SEM-6 was used, and contained several components. The first component of the background current related to the decay of tritium nuclei in the detector chamber is determined by the partial pressure of tritium in the analyzer. The second is caused by the decay of tritium nuclei on the first dynodes of Venetian blind SEM-1 or on the surface of the entrance window of the channel SEM-6. These nuclei arrive at the input of multipliers in the beam of analyzed ions or are sorbed on surfaces in the form of neutral atoms. The third component of the background current caused by the β decay of tritium sorbed on the construction details and walls of the vacuum chamber in the SEM location region depends on the area of details and the system construction.

Because we worked with low partial pressures of tritium in the MRMS analyzer, the first component of the background current was considerably smaller than the second and third ones, depending not only on the partial pressure but also on the time of operation with tritium. Thus, we observed in our instrument [28] for several months a stable background current of $\sim 10^{-16} - 10^{-15}$ A, i.e., exceeding the intrinsic dark current of the photomultiplier by 3–4 orders of magnitude. Approximately the same results were obtained at the same time in [29, 30]. Numerous prolonged heatings of the analyzer at a temperature of $\approx 100\,^\circ$C or above, the 'washing' of the vacuum system with chemically active (O_2, CH_4), inert (He, Ar) gases, and atmospheric air did not, in fact, reduce the background current.

For the precision MRMS measurement of the difference $M(^3\mathrm{T}) - M(^3\mathrm{He})$, the ion beam detector was developed [31, 32], which provided a considerable reduction in the background current caused by the β decay of tritium. The detector is based on the conversion of ions to secondary electrons followed by their conversion to photons detected with a photomultiplier.

The main feature of the detector is the presence of a protective layer deposited on a scintillator. The protective layer protects the scintillator surface from directly incident tritium atoms and molecules and β electrons in the entire ranger of their energies (0 – 18.6 keV) and transmits a considerable fraction of secondary electrons with energies determined by the potential of the target of an ion–electron converter (IEC). This means that the layer thickness should be equal to the maximum penetration depth of ≈ 18.6 keV electrons for the chosen material. The layer should be continuous, without defects, and uniform in width, and its material should have a high adhesion to the scintillator material. In addition, the diffusion of hydrogen isotopes in the protective layer material should be low. After a long search and many experiments, the acid-proof fluorine-containing FP-25 photoresist 6.5 μm in thickness was chosen as a material for the protective layer.

Figure 3 shows schematically an ion beam detector. As an oscillator, a CaF_2(Eu) monolithic screen is used [33]. The target emitter of the IEC has the form of a sphere made of an ShKh-15 high-carbon steel with a cut segment, this flat part being the working surface. The negative potential applied to the target can be continuously varied from 0 to 32 kV. The criterion for the purity of the target surface is the presence or absence of the field emission current when a high negative voltage is applied to the target. An FEU-92 photomultiplier cooled with liquid nitrogen for reducing the intrinsic dark current is used in the detector.

A detailed study of the operation of this ion beam detector showed that the background current of the detector is determined by the intrinsic dark current of the photomultiplier, the possible current of field emission from the target emitter, the background current of cosmic radiation, and a fraction of the background current of β electrons produced in the decay of tritium nuclei on the working surface of the target emitter. These electrons with energies of 30–48.6 keV propagate through the protective layer and probably make the main contribution to the background current.

Studies and measurements also showed that the background current does not exceed 10^{-17} A and the background current of the detector remains constant for a long time. This means that the isotopic exchange of tritium and hydrogen atoms in the FP-25 photoresist proceeds very slowly. Although the developed detector considerably reduced, by at least two orders of magnitude, the influence of background currents caused by the β decay of tritium, this did not allow us to achieve the required accuracy of measuring the mass difference $\Delta M = M(^3\mathrm{T}) - M(^3\mathrm{He})$. The measurement accuracy was a few dozen electron-volts, whereas the measurement accuracy for ion-cyclotron resonance Fourier transform spectrometers [4, 5] did not exceed a few electron-volts.

4. Tritium half-life

In the late 1970s, another problem appeared that could be solved using an MRMS capable of resolving the tritium–helium-3 doublet. The tritium half-life $T_{1/2} = 12.43 \pm 0.05$ year measured in the USA [10] exceeded the value $T_{1/2} = 12.35 \pm 0.03$ accepted in the USSR by 0.08 year (i.e., in fact by a month). Because this characteristic of β decay is necessary for solving a number of scientific and technological problems, such as controllable nuclear synthesis, the β decay theory, the theory of weak and electromagnetic interactions, medical and biological issues, and performing regulated work with devices containing tritium, we began to consider the possibility of measuring $T_{1/2}$ for tritium, the more so since we had already studied tritium earlier and had a few magnetic resonance mass spectrometers with different analytic characteristics.

By that time, about 15 results of measurements of $T_{1/2}$ for tritium had been published. All the measurements were performed by three methods. I will not consider in detail these measurement methods and difficulties inherent in them and will not mention earlier studies of purely historical value, but simply name the methods and attempt to point out the main difficulties inherent in them.

The absolute counting method [10] is based on the measurement of the amount of the decaying parent substance — tritium (11) — while the accumulation method [34] is based on the measurement of the decay product — helium-3. Both these methods require absolute measurements of the substance amount in a sample and, independently of the measurement technique (ionization chamber, mass spectrometer, β spectrometer, or gas balance), it is necessary to prepare reference samples, calibrate measurement devices, accurately measure dividing volumes, control pressure and temperature, and take into account the sorption and diffusion of gases into construction materials of measurement equipment, because experiments can be performed for several years.

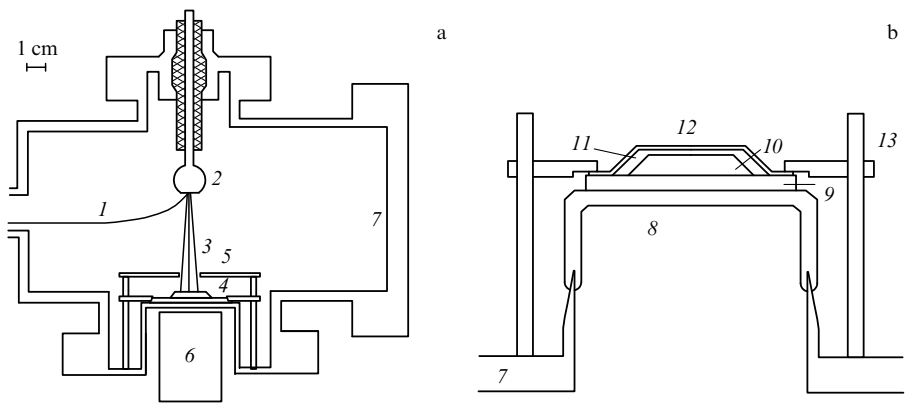

Figure 3. Schematics of a tritium detector (a) and a scintillation unit (b): (*1*) ion beam, (*2*) target of an ion–electron converter, (*3*) secondary electron beam, (*4*) scintillation unit, (*5*) aperture, (*6*) photomultiplier, (*7*) vacuum chamber wall, (*8*) optical window, (*9*) glass substrate, (*10*) monolith CaF_2(Eu) scintillating screen, (*11*) FP-25 photoresist protective layer, (*12*) Al layer, (*13*) clamping attachment.

The third method for measuring $T_{1/2}$ of tritium proposed by Rutherford in 1904 uses microcalorimeters measuring the heat released during the β decay of tritium in a closed volume [35, 36]. This method, called the 'decay curve', reflects in fact the heat release dynamics in time, does not require the measurement of the absolute amount of tritium in a sample, and is devoid of errors caused by diffusion and adsorption, because decay events on surfaces and in the calorimeter material make contributions to the measured quantity. However, other possible errors are inherent in this method which are related, for example, to precision measurements of small temperature variations, the thermostatic control of devices, and accounting for possible chemical reactions of a sample with the calorimeter material. The acquisition of reliable data in such measurements was complicated by the fact that experiments were performed for 10 [35] and even 18 years [36].

In addition, for β decays with a low boundary energy, the probability of electron capturing in the shell of the produced ^{3}He atom is noticeable, and this process is not detected with a calorimeter, because almost all the decay energy is carried away by an antineutrino. The probability of tritium decay with electron capture in the ^{3}He shell can reach about 1% of the total decay probability. The chemical environment of the tritium nucleus also affects the decay probability and the tritium half-life [37, 38]. The influence of these effects on $T_{1/2}$ of tritium was studied in many papers and we will not consider them here. Note, however, that the influence of a chemical medium and of the aggregate state of a tritium sample should be taken into account in accurate measurements of the tritium half-life.

Prolonged studies of the operation of the MRMS with record resolving power during the admission of tritium showed that the background current of the detector prevents the measurement of the absolute amount of substances in gas samples, in particular, tritium or helium-3 with an error smaller than 10%. Such an error was unacceptable for measuring the tritium half-life. For this reason, the method of measuring the tritium half-life in direct experiments by changes in the peak amplitudes of tritium and helium-3 in the sample after long time intervals was rejected, which forced us to consider this problem from a different point of view.

It was proposed in [39] to measure the tritium half-life with the MI-9301 MRMS (or other similar mass spectrometers) with a high absolute sensitivity for $^3He^+$ ($\leqslant 10^5$ helium-3 atoms in the analyzer volume), a resolving power of 10^3 (or higher) at the half-maximum of the mass spectrum line allowing the separation of the $^3He^+$ line from hydrogen ($^1H_3^+$ and $^1H^2D^+$) isotope lines, and a high isotopic sensitivity allowing the measurement of the ratio $^3He^+/^4He^+ \approx 10^{-10}$ and lower by detecting the helium-3 ion current in the photon counting regime.

The method proposed in [39] rules out absolute measurements of tritium and helium-3 amounts in samples and is based on the relative measurements of the $^3He^+/^4He^+$ ratio with the maximum possible accuracy.

Consider several glass ampules filled with a mixture of helium isotopes with the ratio $^3He^+/^4He^+ = R_0$. At the instant t_0, tritium is added to half the ampules, the ampules are sealed off, and all the ampules (control and working) are kept together in liquid nitrogen. According to the radioactive decay law,

$$N = N_0 \exp(-\lambda \Delta t), \tag{12}$$

where N is the number of tritium nuclei decayed for the time Δt, N_0 is the number of tritium nuclei at the initial instant of time t_0, and λ is the decay constant. The amount of ^{3}He produced in the first ampule by the instant t_1 and in the second ampule by the instant t_2 is

$$\Delta^3He^{(1)} = {}^3T_0^{(1)}\{1 - \exp[-\lambda(t_1 - t_0)]\}, \tag{13}$$

$$\Delta^3He^{(2)} = {}^3T_0^{(2)}\{1 - \exp[-\lambda(t_2 - t_0)]\}, \tag{14}$$

respectively, where the decay constant λ is related to the half-life by the expression

$$\lambda = \frac{\ln 2}{T_{1/2}}. \tag{15}$$

By measuring isotope ratios R_{c1} and R_{c2} in control samples without tritium and in working samples with tritium R_{w1} and R_{w2} at instants t_1 and t_2, we find radiogenic additions of helium-3 in samples $\Delta^3He^{(1)}$ and $\Delta^3He^{(2)}$ and use them to calculate part of the decay curve and the tritium half-life from the equation

$$\frac{1 - \exp[-\ln 2(t_1 - t_0)/T_{1/2}]}{1 - \exp[-\ln 2(t_2 - t_0)/T_{1/2}]} = \frac{R_1}{R_2}, \tag{16}$$

where $R_1 = R_{w1}/R_{c1} = {}^3He^{(1)}/{}^4He^{(1)}$ and $R_2 = R_{w2}/R_{c2} = {}^3He^{(2)}/{}^4He^{(2)}$ are isotope ratios measured in the first and second ampules at instants t_1 and t_2. In general, transcendent equation (16) for $T_{1/2}$ is solved numerically. However, particular cases exist in which solutions can be obtained analytically for $\Delta t_2 = 2\Delta t_1$ and $\Delta t_2 = 3\Delta t_1$.

Obviously, the reconstruction of the exponential decay curve by two experimental points obtained in 1–2 years for a half-life exceeding 12 years can introduce considerable errors into the determination of $T_{1/2}$ of tritium. Therefore, either such measurements should be performed for many years or the number of points on the decay curve should be greater. In any case, it is necessary to perform a series of control measurements in such experiments, which would confirm the absence of considerable systematic errors in this procedure.

The half-life of tritium was measured with an MRMS (Fig. 4) with a record high absolute sensitivity for helium-3 ($\leqslant 10^5$ atoms in the mass analyzer volume) [40, 41] operating in the double-beam regime, which allows the simultaneous measurement of the $^3He^+$ and $^4He^+$ ion currents. The double-beam operation regime of the mass spectrometer means that $^3He^+$ and $^4He^+$ ions are simultaneously produced in the ion source, escape from it with the same energy, and, according to Eqn (4), move along orbits with different radii. The $^4He^+$ ions fly by a lager radius, pass almost a half turn in the magnetic field, enter the collector C($^4He^+$), and are detected with an electrometric amplifier. This part of the instrument can be considered a static magnetic sectorial mass spectrometer with a low resolving power and high sensitivity. To obtain the high sensitivity, the width of the exit slit S_0 of the ion source was set to about 2 mm. The width of the slit S_3 in front of the ion collector was approximately the same. The resolving power of this stage of the instrument was about 20, which is sufficient for separating helium isotopes. The helium-3 ions escaping from the source with the same energy as $^4He^+$ ions move along an orbit with a smaller diameter, enter the modulator M, and are separated from $^1H_3^+$ and $^1H^2D^+$ ions in the high resolution stage with a MRMS. This stage of the instrument operates in the compensation regime, which, as shown above,

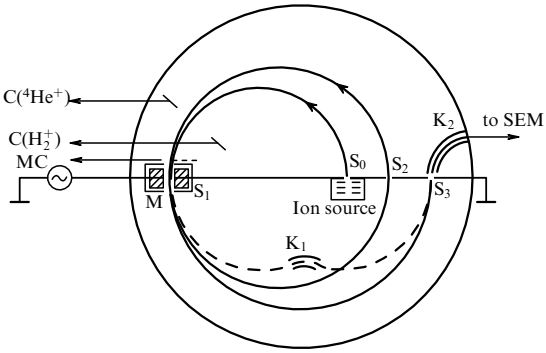

Figure 4. Schematic of the double-beam MRMS-9301. S_0: exit slit of the ion source, S_1: slits in electrodes of modulator M, S_2: drift slit, S_3: exit slit of the analyzer, K_1: deflecting capacitor, K_2: ejecting capacitor, MC: high-frequency generator, C(H_2^+): collector for molecular hydrogen ions, C(^{4}He$^+$): collector of helium-4 ions.

provides a higher sensitivity than the resonance regime. The absolute sensitivity of the MRMS is also increased in the regime of static evacuation of the mass analyzer [42], when, after the admission of the sample under study, the working pressure in the analyzer ($10^{-8}-10^{-7}$ Torr) is maintained by a sorption pump in which a titanium mirror cooled by liquid nitrogen is used as a getter.

Before putting the working sample into the MRMS analyzer, the tritium should be separated from the helium isotopes. This is performed by passing the sample through a palladium membrane heated to 500–600 °C. The instants of gas passing through the membrane are denoted by t_1, t_2, t_3, etc. The time of tritium passing through the membrane not exceeding 5 min does not introduce a noticeable error into the final result. The separated tritium is collected by sorption in activated carbon at liquid nitrogen temperature.

This method of measuring the tritium half-life $T_{1/2}$ [39] was realized at the mass spectrometry laboratory at the PTI [43, 44]. Two variants of experiments were performed: with and without calibration measurements of blank samples without tritium. In the method with calibration mixtures, four series of measurements were performed for $t_1 =$ 243.06 days, $t_2 = 460.02$ days, $t_3 = 488.2$ days, and $t_4 =$ 585.97 days and the result $T_{1/2} = 12.296$ years was obtained for gaseous tritium. The duration of the solar year was taken to be 365.25 days. In the method without calibration, two series of measurements for $t_5 = 663.99$ days and $t_6 =$ 846.06 days gave the half-life $T_{1/2} = 12.273$ years.

The weighted mean half-life of gaseous tritium was $T_{1/2} = 12.279$ years.

The root-mean-square errors for individual measurement series were $(2-7)\times 10^{-5}$. The authors of [43, 44] estimated possible systematic errors of experiments caused by gas losses in samples during ampule sealing, the dissolving of helium isotopes in the ampule glass, etc. The total measurement error was 0.033 year and the final result of measurements was [43]

$$T_{1/2} = 12.279 \pm 0.033 \text{ years} \quad (\pm 0.27\,\%)\,.$$

Thus, the mean value of the half-life of molecular tritium measured by the proposed helium-isotope method is in good agreement with the results obtained in other studies. The measurement error of $T_{1/2}$ was $\approx 0.27\%$, and analysis of experiments did not reveal any new error sources not predicted earlier.

5. Studies of tokamak construction materials with a magnetic resonance mass spectrometer

Another application of the MRMS having high absolute sensitivity concerns the study of the interaction of a deuterium plasma with the construction materials of tokamaks and the estimate of the formation rate of products of nuclear synthesis reactions for the plasma parameters achieved. The spherical Globus-M tokamak belongs to a new generation of magnetic setups that can provide better plasma parameters than those in conventional toroidal tokamaks of the same size [45].

The Globus-M is intended for studying physical processes in plasmas and the development of engineering designs of spherical tokamaks with plasma currents up to 1 MA (10^6 A). The results of such studies are of direct interest for the International Thermonuclear Experimental Reactor (ITER) project, because experiments are performed in a broad range of parameters.

The use of a deuterium plasma allows the simulation of the future operation of tokamaks with the deuterium–tritium cycle, the study of the physics of proceeding processes, the investigation of construction materials, and the development of methods and equipment for the diagnostics of plasma parameters and their control.

The burning of a deuterium plasma in a tokamak chamber can involve two nuclear synthesis reactions with the production of a light helium isotope and a heavy hydrogen isotope (tritium):

$$^2\mathrm{D} + {}^2\mathrm{D} \to {}^3\mathrm{He}\,(0.82\ \mathrm{MeV}) + \mathrm{n}\,(2.45\ \mathrm{MeV})\,, \tag{17}$$

$$^2\mathrm{D} + {}^2\mathrm{D} \to {}^3\mathrm{T}\,(1.0\ \mathrm{MeV}) + \mathrm{p}\,(3.02\ \mathrm{MeV})\,, \tag{18}$$

their probabilities being virtually the same. This means that, if we are able to measure the amount of helium-3 produced, we can state that approximately the same amount of tritium atoms, protons, and neutrons are produced during the nuclear synthesis [46].

The cross sections ($\sim 10^{-25}$ cm^2) for reactions (17) and (18) achieve the maximum for electron energies of $\sim 10^3$ keV. Because the electron temperature of plasma in the Globus-M tokamak achieved at present does not exceed 0.6 keV, the cross sections for reactions (17) and (18) are roughly estimated as $\sim 10^{-36}$ cm^2. Thus, the probability of a nuclear synthesis reaction in the deuterium plasma of the Globus-M tokamak has been very low so far. Therefore, it seems impossible to estimate by the known methods the absolute numbers of particles (protons, neutrons, tritium and helium-3 atoms) produced in these synthesis reactions in the tokamak chamber. In this paper, we will not discuss the methods of detecting the extremely weak fluxes of elementary particles (protons and neutrons), but briefly consider the methods for detecting tritium.

The radiometric method for detecting tritium and measuring the amount based on β electron counting with the help of gas-filled or liquid scintillation counters uses decay formula (11) and radioactive decay law (12). The known parameters of the tritium decay (tritium nucleus half-life $T_{1/2} \approx 12.3$ year $\approx 4\times 10^8$ s, average β electron energy $E_{\mathrm{av}} \approx$ 5.6 keV, maximum energy $E_{\max} \approx 18.6$ keV, and energies 0–5 keV of more than 50% β electrons produced in tritium decay) characterize the sensitivity of these counters. To reliably detect β decay events, a gas sample should contain

$\geqslant 4 \times 10^8$ tritium atoms because the half-life $T_{1/2} \approx 4 \times 10^8$ s assumes that one β decay occurs per second (in the first approximation). For a more reliable detection to obtain the representative statistics, the number of tritium atoms in the sample should be $\geqslant 10^9$.

As mentioned a few times above, the sensitivity of magnetic resonance mass spectrometers developed at PTI is $\sim 10^5$ (and lower) helium-3 atoms in a sample [47], i.e., the MRMS sensitivity for helium-3 is at least four orders of magnitude higher than the sensitivity of the radiometric method for detecting tritium. Note here that the ^{4}He isotope is mainly the decay product of transuranium elements, while the ^{3}He isotope is the synthesis product of deuterium nuclei (18) or the decay product of tritium nuclei (11). Therefore, the measurement of the ratio ^{3}He/^{4}He of the amounts of helium isotopes and their variations in time can give information on the dynamics of natural and technogenic processes.

Note also that the volume content of ^{4}He in air is $\approx 5.2 \times 10^{-4}$% and the ratio of helium isotopes in Earth's atmosphere, ^{3}He/^{4}He $\approx 1.4 \times 10^{-6}$, is a peculiar constant. Helium isotope ratios measured in experiments with helium isotopy are compared namely with this value [48], independently of the nature of samples under study.

The method for separation and purification of helium isotopes from chemically active and heavy inert gasses in solid, liquid, and gaseous samples is well developed and described in detail in the literature [48, 49] and, therefore, we will not consider it here. Note only that samples for studies were construction materials that had been in the vacuum chamber of the Globus-M tokamak for a long time: a fragment of a stainless steel grid (sample no. 1), a sheet of stainless steel (no. 2), quartz sight glass (no. 3), and dust from the bottom and walls of the chamber (no. 4).

Because the 'washing' and clearing of the vacuum chamber after its opening for repair or modification were performed by filling it with a heavy helium isotope up to pressures of a few Torr followed by evacuation, heating, and gas discharge burning, it was reasonable to assume that the content of ^{4}He in samples will be very high. Commonly, grade 60 high-purity helium-4 was used in which the certified volume fraction of impurities (nitrogen, oxygen, argon, methane, hydrogen, neon, water vapor) did not exceed 2×10^{-4}%, but the amount of the light ^{3}He isotope was not indicated. It is known from the literature [48] that the isotope ratio in helium tanks is ^{3}He/^{4}He $\approx 2 \times 10^{-8}$. Our control measurements of the isotope ratio gave the value of ^{3}He/^{4}He $\approx (3.9 \pm 1.0) \times 10^{-8}$. The assumption about the high content of the heavy helium isotope in the construction materials of the tokamak was confirmed already in the first measurements. For this reason, the mass of samples under study was reduced to a few milligrams to decrease the amount of extracted ^{4}He and avoid memory effects in the filling system and mass spectrometer analyzer. Gases captured in the sample material escaped during sample heating up to high temperatures (up to 1300 °C) in corundum crucibles of a special reactor [50, 51]. The number of helium isotopes escaped from samples was measured in known units of 1 pv $\approx 3.5357 \times 10^{13}$ atoms, corresponding to the number of gas atoms in a volume 1 mm^3 at a pressure of 1 Torr.

Table 1 presents isotopic ratios ^{3}He/^{4}He and contents of ^{4}He measured in samples with different masses and the calculated contents of ^{3}He and ^{4}He in 1 g of samples. Each measurement cycle of isotope ratios was performed using the technique blank–reference–measured–reference samples. As the blank sample, gas from the reactor in the absence of any material in the crucible was used. Reference samples were gas mixtures with isotope ratios close (within an order of magnitude) to these ratios in the samples under study. In all measurements, the mass spectrometer operated in the double-beam regime. The measurements of ^{3}He were performed in the MI-9301 high resolving power regime. Each measurement included from six to eight recordings of the mass peak, and these results mainly determined the measurement error because the ^{4}He peak, which usually was very intense, was detected in the low-resolution regime with a small error. In measurements of samples 1 and 4, the amounts of ^{4}He were anomalously high. Therefore, to ensure the standard operation of the mass spectrometer, it was necessary to reduce the amount of the extracted gas by several orders of magnitude. The accurate division of the extracted gas and the determination of the selected ratio were rather complicated during measurements, and therefore the total amount of the extracted helium was estimated from the gas pressure in the reactor volume. The error of this measurement procedure was rather high, about 30%, according to our estimates.

It can be seen from Table 1 that the ^{3}He/^{4}He isotope ratios measured for samples 1, 2, and 4 lie within $(1.6–4.3)\times10^{-7}$, i.e., an order of magnitude higher than the isotope ratio of helium in tanks and an order of magnitude lower than the isotope ratio for atmospheric helium. As for ^{4}He, its anomalously large amounts in samples can be explained by the fact that ^{4}He$^+$ ions penetrate construction materials during the gas discharge washing of the vacuum chamber and during plasma discharges. In addition, ^{4}He$^+$ remains in slits between pats, microcracks in materials, and other narrow spaces from which vacuum pumping after chamber washing is hampered.

It would seem that isotope ratios obtained in our measurements with samples can be explained by two processes. First, atmospheric ^{4}He could enter the tokamak chamber during its depressurization and during sampling and storage of helium in tanks used for washing. Second, helium isotope ratios in samples could be determined by the formation of ^{3}He in reactions (11) and (18). However, the results of calculations show that the dilution of tank helium by half in volume by air changes the isotope ratio by only a

Table 1. Isotope ratios and content of helium isotopes in samples.

Sample number	Weighed portion, mg	^{3}He/^{4}He in the sample	^{4}He in the sample, pv	^{3}He in the sample, pv	^{4}He in the substance, number of atoms per g	^{3}He in the substance, number of atoms per g
1	0.5	$2.5 \times 10^{-7} \pm 14$ %	$1.5 \times 10^3 \pm 30$ %	3.7×10^{-4}	1.1×10^{20}	2.7×10^{13}
2	1.4	$4.3 \times 10^{-7} \pm 10$ %	1.7 ± 5 %	7.3×10^{-7}	4.2×10^{16}	1.6×10^{10}
3	1.9	$2.2 \times 10^{-6} \pm 2$ %	0.45 ± 7 %	1.0×10^{-6}	8.3×10^{15}	1.8×10^{10}
4	7.1	$1.6 \times 10^{-7} \pm 2$ %	$1.2 \times 10^4 \pm 30$ %	1.9×10^{-3}	6.0×10^{19}	9.5×10^{12}

few fractions of a percent. The first assumption is also completely rejected by the fact that the absolute amounts of ^{3}He in samples are anomalously large ($\sim 10^{13}$ atoms for every 1 g), which is several orders of magnitude greater than the maximum content of the light helium isotope in natural and technogenic samples measured earlier for almost 40 years. For example, this quantity is three orders of magnitude higher than in metals: different brands of steel, aluminum, and silver; and two orders of magnitude higher than in dust in a laboratory where work with tritium was performed earlier. Thus, the only explanation for the obtained isotope ratios $^3\mathrm{He}/^4\mathrm{He} \sim 10^{-7}$ and large absolute amounts of ^{3}He in sample nos 1 and 4, in our opinion, is the synthesis of ^{3}He and tritium decay. As for stainless steel (no. 2) and quartz (no. 3) samples, the content of ^{3}He in them, although rather high (10^{10} atoms per g), could not allow us to make a certain conclusion about the source of the light helium isotope.

To find the distribution of sorbed helium in a sample, we measured the helium isotope ratio in the step heating of sample no. 5 identical to sample no. 1. The sample was first heated to 300 °C, and the complete cycle of purification and measuring the isotope ratio of extracted helium isotopes was performed. Then such measurements were performed by heating the sample to 500, 700, 900, and 1100 °C. Measurements showed that upon heating the sample from 20 °C to 300 °C, the isotope ratio of the extracted gas was somewhat lower than that in the temperature ranges of 300–500 °C and 500–700 °C. This can mean that the amount of ^{3}He contained on the material surface is slightly higher than in the sample volume. The total amount of ^{3}He extracted from sample no. 5 upon step heating virtually coincided with the amount of gas extracted from sample no. 1.

The generation rate of helium-3 and tritium can be estimated from the known number of deuterium plasma discharges and their durations. In the case under study, the number of discharges between the openings of the tokamak vacuum chamber before the selection of samples and dust was $\approx 10^4$ for the average discharge duration of ≈ 0.1 s. Therefore, the generation rate achieved for helium-3 and tritium in the Globus-M tokamak per 1 g of material for temperatures of 500–600 eV is $10^7 - 5 \times 10^9$ nuclei per 1 s or 10^6–5×10^8 nuclei per discharge. It seems that the estimate of total amounts of produced ^{3}He and ^{3}T and proton and neutron fluxes is impossible because of the difficulty of estimating the mass of construction materials of the Globus-M tokamak and distributions of these gases over the depth of their penetration into materials.

A more systematic approach to the choice of samples of materials used in tokamaks from the point of view of their composition, location in the chamber, irradiation time, and contact time with plasma can probably give important qualitative and quantitative data on interaction processes between deuterium plasma and construction materials of tokamaks and other plasma setups.

6. Time-of-flight mass spectrometers

The second type of mass spectrometer, which was developed at the PTI, gained international recognition, and is widely used in many fields of science and technology, is the nonmagnetic time-of-flight mass spectrometer with a reflector, which was called the mass reflectron by its creators.

Before discussing the design and parameters of these instruments, we consider briefly the design of their predecessors — linear time-of-flight instruments [52–54]. The concept of the latter is very simple. An ion source consists of three plane-parallel grids making two gaps. Corresponding potentials are applied to the grids. Ions produced in the first gap by a pulsed electron beam are ejected perpendicular to the electron beam direction to the second gap, where they are accelerated to the energy qU (where q is the ion charge and U is the potential difference between grids forming the second gap of the source). Having escaped from the source, ions move in the drift space towards a detector. During their motion, ions are separated according to the mass/charge ratio M/q: light ions, escaping from the source with higher velocities, pass through the drift space faster and are the first to reach the detector, whereas the heaviest ions are the last. By equating the electric field energy qU to the kinetic energy of ions and expressing the velocity of particles in terms of the trajectory length and motion time, we obtain the expression

$$T = L\left(\frac{M}{2qV}\right)^{1/2} \tag{19}$$

for the motion time of ions from the source to detector, where L is the distance between the source and detector. It follows from (19) that the resolving power of such an instrument based on the peak is described by the expression

$$R = \frac{M}{\Delta M} = \frac{T}{2\Delta t}\,, \tag{20}$$

where Δt is the time interval during which ions with the same ratio M/q arrive at the detector. The time Δt is determined by the 'thickness' (duration) of ion packets at the detector input consisting of ions with the same mass/charge ratio.

It follows from Eqns (19) and (20) that the resolving power of linear time-of-flight mass spectrometers is directly proportional to the time of flight of ions through the drift region, i.e., to the instrument length, and is proportional to the square root of the ion mass. The latter circumstance was ignored, as a rule, because studies were usually performed in the range of middle mass numbers from 20 to 100 a.m.u. As for the ion packet duration Δt, it depends on many factors [54–56]: the initial thermal dispersion of ionized gas molecules in the source in magnitude and direction, the dispersion of kinetic ion energies in the electron impact ionization, the nonequipotential nature of ion creation sites in the ionization chamber of the source, the duration of an electric field pulse in the source, the influence of the volume charge field in ion packets, the expansion of packets during their drift, etc. Thus, the resolving power depends on all aberrations of the instrument.

For a drift length of about 1 m, the resolving power of linear time-of-flight mass spectrometers in the region of middle mass numbers (20–100 a.m.u.) does not usually exceed 100, while in the region of light masses (2–20 a.m.u.) it was about 50 [54, 56], which considerably restricted their applications. Nevertheless, these instruments have a number of advantages over other types of mass spectrometers:

(i) the fast operation (the total spectrum in the entire mass range can be obtained for one pulse ejecting ions from the source, i.e., for fractions of a second);

(ii) the unlimited mass range (all ions produced in the source reach the detector and are detected);

(iii) the high sensitivity (a large ionization volume and the absence of aperture slits);

(iv) the possibility of recording spectra in different regimes (in the usual regime, the entire spectrum is recorded,

while in the synchronous regime, separate mass lines or groups of lines are recorded).

All the above only emphasizes the importance of efforts devoted to increasing the resolving power of time-of-flight instruments.

The idea of increasing the resolving power of a time-of-flight mass spectrometer was reported for the first time in [57]. The author of [57] proposed the multiple reflection of ions with the help of reflectors located at opposite ends of a mass analyzer of a certain length (≈ 0.5 m). After a great number of cycles (several hundred), when ions with close ratios M/q are separated, they are deflected and detected. The author of [57] also proposed the idea of compensation of the ion energy dispersion (and, hence, of the time of flight) in reflecting gaps. This paper [57] was theoretical: only the idea was explored and no technical details or the instrument design were considered in it. The paper did not initiate any practical development and probably was unnoticed by experimenters because, until recently, no references to it appeared.

7. Mass reflectron with the V-shaped ion trajectory

Within 10 years of the publication of S G Alikhanov's paper [57], the invention was patented [58] and the development of a time-of-flight mass spectrometer was started at the PTI, which was later called the Mamyrin mass reflectron [59, 60].

Figure 5 shows schematically a time-of-flight mass spectrometer (TFMS) with a two-gap reflector. One can see from the figure that ions have the V-shaped trajectory. Such a trajectory at once imposes strict conditions on the design and size of the instrument because, for an analyzer length of about 1 m, the angle α is $\approx 2-3°$, and therefore the diameter of the vacuum chamber of the analyzer should be no less than 0.18 m. As in the linear TFMS considered in Section 6, ions escape from the pulsed source I in the form of plane packets with a certain energy and are deflected by the angle α in the direction to the analyzer axis with the help of deflecting plates or the fourth grid electrode placed at the angle α with respect to three other electrodes. The ions move in the nonfield drift space L_1 to reflector RS. The reflector consists of two transparent plane–parallel grids and a solid electrode, which form two plane gaps d_T and d_K. All the electrodes are under the corresponding potentials. Ions lose a considerable part of their energy in the first braking gap d_T and their velocity vanishes in the second gap d_K. They change the direction of motion to the opposite one, are accelerated in the field of the first gap d_T, move in the nonfield space L_2, arrive at the input of an SEM, and are detected.

The specific feature of the operation of the mass reflectron [59, 60] is that it provides compensation for the difference in the times of flight through nonfield drift regions L_1 and L_2 for ions with the same ratio M/q, which is caused by the ion energy spread in the source. The reflector with two gaps allows the second-order focusing required for achieving a high resolving power at a large ion energy spread to be obtained.

As with any TFMS, the resolving power of the mass reflectron is described by Eqn (20). To calculate the total time T of the motion of ions in the instrument, the trajectory is divided into individual parts, with ions being subjected to the action of one potential in each of them. The mass spectrometer considered here contains five such regions. All the stages of calculation of the time of flight of an ion from the source to the detector are described in detail in original papers [60, 61]. Therefore, we present here only the final expressions required for further analysis,

$$T = CF(k)\,, \tag{21}$$

$$F(k) = \frac{A_1}{k^{1/2}} + nA_1\left[k^{1/2} - (k-p)^{1/2}\right] + (k-p)^{1/2}\,, \tag{22}$$

where

$$A_1 = \frac{L}{4d_K}\frac{U_K}{U_0}\,, \quad n = \frac{4d_T}{L}\frac{U_0}{U_T}\,, \quad p = \frac{U_T}{U_0}\,,$$

$$C = \frac{4d_T}{(2qU_0/M)^{1/2}}\frac{U_T}{U_K}\,. \tag{23}$$

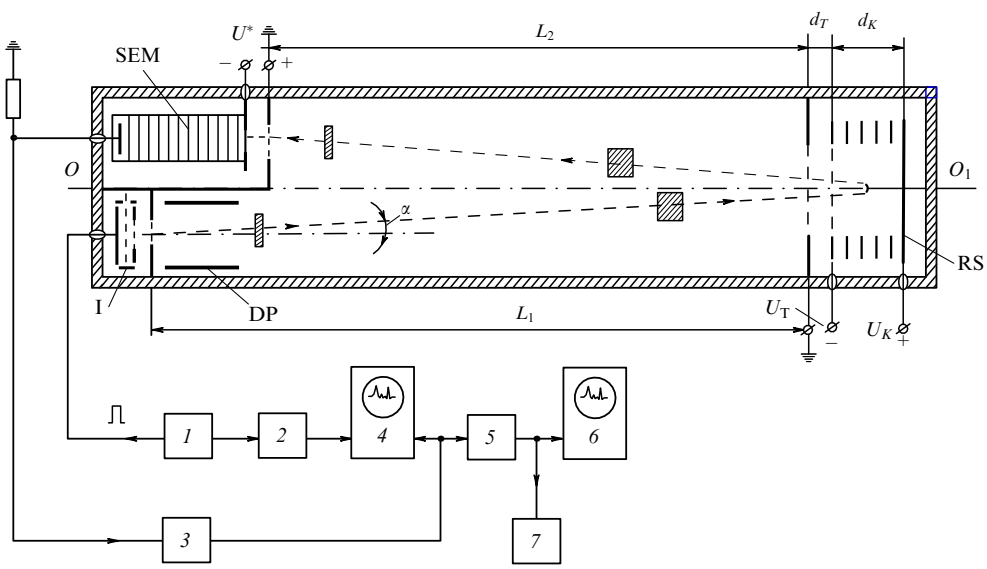

Figure 5. Schematic of a time-of-flight mass spectrometer (mass reflectron) with the V-shaped ion trajectory: (I) ion source, (DP) deflecting plates, (RS) reflector, (*1*) rectangular pulse generator, (*2*) delay line, (*3*) broadband amplifier, (*4*) broadband oscilloscope, (*5*) stroboscopic attachment, (*6*) oscilloscope, (*7*) electronic potentiometer.

Here, notations presented in Fig. 5 are used; qU_0 is the average ion energy corresponding to their velocity along the system axis; $qU = kqU_0$ is the energy of any ion, $k = U/U_0$, $k \approx 1$; L is the total length of the nonfield drift space; d_T is the braking gap width; and d_K is the reflecting gap width. Constants A_1, n, p, and C are independent of k.

Focusing conditions for the time of flight in the second-order energy have the form

$$\frac{\mathrm{d}T}{\mathrm{d}U} = 0 \text{ at } U = U_0\,, \quad \frac{\mathrm{d}^2T}{\mathrm{d}U^2} = 0 \text{ at } U = U_0\,. \tag{24}$$

These conditions in a more convenient form can be written as

$$\left.\frac{\mathrm{d}F}{\mathrm{d}k}\right|_{k=1} = 0\,, \quad \left.\frac{\mathrm{d}^2F}{\mathrm{d}k^2}\right|_{k=1} = 0\,. \tag{25}$$

Taking into account that U_0 and U_t are comparable and the braking gap length d_T is much smaller than the drift space L_1 or L_2, we can assume that $n \ll 1$. By equating the first and second derivatives from F to zero and solving the equations obtained, we find the quantities

$$p \approx (3)^{1/2}\,, \quad A_1 \approx \frac{2}{3}\,, \quad F_0 = F|_{k=1} \approx \frac{4}{(3)^{1/2}}\,, \tag{26}$$

which, together with (23), allow us to calculate the main geometrical and electric parameters of the mass reflectron. As for calculating the resolving power of the TFMS, it follows from (20) that this requires knowledge of the duration Δt (thickness Δl) of ion packets with the same ratio M/q at the detector input. The quantity Δt includes several terms, the main one determined by the initial ion energy spread in the source, and it cannot be expressed analytically.

However, the resolving power of the TFMS bases on the peak can be estimated [59] based only on the inaccuracy of focusing the time of flight of ions when changing their energy:

$$R_U = \frac{T}{2(T - T_0)} = \frac{F_0}{F - F_0}\,, \tag{27}$$

where T_0 is the mean time of flight through the entire trajectory. Be expanding the difference $F - F_0$ in a Taylor series in powers of the small energy increment $\delta = (U - U_0)/U_0$ in the vicinity of $k = U/U_0 = 1$, we obtain from expressions (22), (26), and (27)

$$R_U = \frac{4.6}{\delta^3 - 3.1\,\delta^4}\,. \tag{28}$$

In fact, δ determines the ion energy spread with respect to the mean energy. By substituting the different values of $\delta < 1$ into (28), we can estimate the maximum resolving power that can be achieved in the region of high mass numbers. One of the peculiarities of this instrument is that a permanent magnet can be introduced to the ion source for ion beam focusing to diminish the ionization zone and the ion packet thickness, thereby increasing the resolving power of the mass reflectron [62]. After numerous modernizations and adjustments, the resolving power of the instrument by the peak half-maximum was $R_{50\,\%} \geqslant 5 \times 10^3$ in the region of 700 a.m.u. and above; for $M/q \geqslant 200$ a.m.u., $R_{50\,\%} \approx 3 \times 10^3$, and in the region of light ions (3–4 a.m.u.), $R_{50\,\%} \leqslant 400$. This instrument was widely used for studying fullerenes [63], metallofullerenes [64], and various heavy ions [65].

8. Linear mass reflectron

One of the disadvantages of the mass reflectron with the V-shaped ion trajectory considered in Section 7 is the rather large diameter of the cylindrical vacuum chamber, because the source and detector are located at one end of this cylinder. This circumstance considerably increases the size and weight of the instrument and prevents its use for solving a number of problems. Because of this, after many calculations and experiments, a new ion-optical scheme of a time-of-flight spectrometer with an ion reflector was proposed, which was called a linear mass reflectron [66].

Figure 6 shows a schematic of this instrument. Ions move along trajectories parallel to the analyzer axis. Ion packets are formed as follows. Ions produced in electron impacts in the ionization gap d_1 are ejected from it by a rectangular voltage pulse U_1, accelerated in the first accelerating gap d_5, fly through the first nonfield drift region L_1, are decelerated and reflected in the reflector (gaps d_3 and d_4), fly through the drift region L_1 and source in the opposite direction, fly through the gap d_2 and the second drift region L_2, and fall on the detector. The total time of flight of ions from the source to detector can be divided into two parts: the time of flight T_1 in the reflector and the time of flight T_2 in all other regions. The ions with the same ratio M/q but with higher energies spend a shorter time passing through the entire path, except the reflector, than the same ions with lower energies. However, higher-energy ions penetrate deeper into the reflector and reside in it for a longer time than lower-energy ions. It is necessary to select reflector parameters so that the total time of flight $T = T_1 + T_2$ of ions with the same ratio

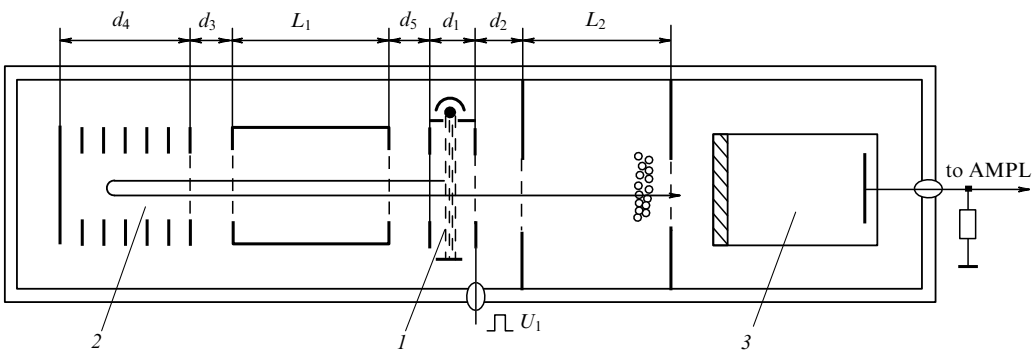

Figure 6. Schematic of a mass reflectron with linear ion trajectory: (*1*) two-gap ion source, (*2*) reflector, (*3*) detector, (AMPL) broadband amplifier in the detection system, (U_1) ejecting pulse amplitude in the ion source, (d_1 and L_1) gap lengths between analyzer elements.

M/q from the source to detector would be weakly dependent on their energy. Then, ions of the same kind will arrive at the detector input in the form of a short (thin) packet, which is necessary to obtain the high resolving power.

As with any TFMS, the resolving power of a linear mass reflectron is described by expression (20). The important difference between it and the instrument with the V-shaped ion trajectory is that the number of independent regions of motion and potentials in the linear mass reflectron is much greater (see Fig. 6). Therefore, the number of terms in the expression for the total time of flight becomes equal to 11:

$$T=\left(\frac{M}{2q}\right)^{1/2}\left\{\frac{2d_1}{U_1}\left(\frac{U_1x}{d_1}\right)^{1/2}+\frac{2d_2}{U_2}\left[\left(\frac{U_1x}{d_1}+U_2\right)^{1/2}-\left(\frac{U_1x}{d_1}\right)^{1/2}\right]+\frac{4d_3}{U_3}\left[\left(\frac{U_1x}{d_1}+U_5\right)^{1/2}-\left(\frac{U_1x}{d_1}+U_5-U_3\right)^{1/2}\right]+\frac{4d_4}{U_4}\left(\frac{U_1x}{d_1}+U_5-U_3\right)^{1/2}+\frac{4d_5}{U_5}\left[\left(\frac{U_1x}{d_1}+U_5\right)^{1/2}-\left(\frac{U_1x}{d_1}\right)^{1/2}\right]+\frac{2L_1}{(U_1x/d_1+U_5)^{1/2}}+\frac{L_2}{(U_1x/d_1+U_2)^{1/2}}+\frac{d_1}{(U_1x/d_1)^{1/2}}\right\}, \quad (29)$$

where d_i and U_i are distances and potential differences between the electrodes of corresponding gaps and x is a part of the ion trajectory in the ionization chamber of the source.

The duration Δt of ion packets at the detector input is mainly determined by the initial energy spread ΔU and parameters of the ionization chamber,

$$\Delta t=\frac{4d_1}{U_1}\left(\frac{M\Delta U}{2q}\right)^{1/2}, \quad (30)$$

where d_1 is the width of the ionization chamber of the source, U_1 is the amplitude of the ejecting pulse, and q and M are the ion charge and mass, respectively. It can be seen from (30) that the increase in the ejecting pulse amplitude U_1 and decrease in the width d_1 of the ionization chamber of the ion source reduce the duration of ion packets at the detector input and increase the resolving power of the linear TFMS. After numerous calculations, the optimization of geometrical and electric parameters, and prolonged studies of the instrument, its creators have managed to obtain $R_{50\,\%}=1200$ in the mass region 300–350 a.m.u. for a vacuum chamber length of 0.9 m and an inner diameter of the chamber of 60 mm.

The linear mass reflectron has a lower resolving power than that of the mass reflectron with the V-shaped ion trajectory with the same mass analyzer length (because of a shorter ion trajectory) and a lower sensitivity due to a large number of grids separating different parts of the trajectory through which the ion beam propagates. However, many advantages inherent in time-of-flight instruments, such as fast operation, an unlimited mass range, and the possibility of detecting ion currents in different regimes, as well as their compactness, simplicity, and rather low cost, make linear mass reflectrons irreplaceable for control of complex technological processes [67] and the development of small devices for studying the upper atmospheric layers [68] and possibly the internal atmosphere of space stations and spacecraft.

9. Analysis of tritium-containing fuel gas mixtures with a linear mass reflectron

One of the important problems in the creation of a thermonuclear reactor, in particular, ITER, is the development of an on-line method for chemical and isotopic analysis of deuterium–tritium gas mixtures for use as a fuel. Except the main components — deuterium and tritium — fuel mixtures may contain impurities: H_2, ^3He, ^4He, O_2, and oxides of different elements, hydrocarbons, nitrogen and its compounds, etc. The concentration range of impurities can be very large, from 10^{-5} to 5%.

Fuel gas mixtures in thermonuclear facilities are usually analyzed with quadrupole or omegatron mass spectrometers and double-focused static magnetic instruments. The common feature of these instruments is the continuous operation of their detecting systems. As long as studies of tokamaks are performed with a deuteron plasma, such mass spectrometers can be used to analyze impurities in deuterium and plasma combustion products. In fuel mixtures containing tritium, the background currents of detectors in such mass spectrometers can increase by a few orders of magnitude, as pointed out in [7, 28], which prevents the measurement of not only impurities in gas mixtures but also the main components.

The authors of [69] proposed that tritium-containing gas mixtures be analyzed with a time-of-flight mass reflectron with the ion source and detector operating in the pulsed synchronous regime with the accumulation of ions during the pause T between pulses. Because the time noise distribution caused by the β decay of tritium atoms is uniform and the noise current is proportional to the ratio τ/T (τ is the duration of a pulse opening the detector), the shorter τ is, the smaller the contribution of the noise current to the output signal. The upper estimate of one of the components of the noise current can be obtained assuming that a monolayer cover, for example, of a microchannel plate ≈ 10 cm^2 in area contains 10^{15} tritium atoms per cm^2. Taking into account that the tritium half-life is $T_{1/2}\approx 12.3$ years $\approx 4\times 10^8$ s, we obtain the background current during the work pulse duration $\tau\approx 2\times 10^{-8}$ s at ≈ 0.5 pulse per s. At the same time, the number of ions in the useful signal packet can be from a few units to a few thousand, depending on the sample composition, its pressure, the instrument adjustment, etc.

To test this proposal, a mass reflectron with a linear ion trajectory ≈ 180 mm in length was used. The analyzer length was ≈ 240 mm, the resolving power in the region of light ions (3–4 a.m.u.) was $R_{10\,\%}\approx 50-60$, the sensitivity by the partial pressure of Ar was $\approx 10^{-11}$ Torr, the range of measured masses was 1–150 a.m.u., and the detection time of 20 gas components was ≈ 1 s. The main task of experiments was to record the molecular tritium $^3T_2^+$ peak and to study the influence of the background current of the detector on errors in measurements of line intensities in mass spectra during prolonged experiments with tritium.

Before the main measurements, the mass spectrometer was adjusted to the $^1H^+$, $^1H_2^+$, $^4He^+$, $^{14}N^+$, $^{16}O^+$ lines for an residual pressure in the analyzer of $\approx 10^{-8}$ Torr and then operated in the automatic regime. After the admission of a tritium sample (count time t_0) up to a pressure of $\approx 7\times 10^{-7}$ Torr, the intensities of these peaks barely changed, except the peaks of atomic and molecular protium, and the unresolved peak of $^3T^+-{}^3He^+$ and the peak of molecular tritium $^3T_2^+$ appeared in the spectrum. Because the gas under

Table 2. Intensities of peaks of residual gasses in the TFMS analyzer during the admission of tritium depending on the exposure times.

Measured ions	Intensity of peaks at different times				Measurement error, %
	t_0	$t_1 = 40$ min	$t_2 = 80$ min	$t_3 = 120$ min	
$^1H^+$	15	17	20	23	0.2
$^1H_2^+$	174	204	214	203	0.2
$^3T^+ + {}^3He^+$	1001	910	894	1045	0.4
$^4He^+$	44	40	39	51	0.1
$^3T_2^+$	306	284	280	307	0.2
$^{14}N^+$	46	54	56	57	0.2
$^{16}O^+$	45	59	63	52	0.2

study was admitted to the analyzer from a small measuring volume (about 0.5 cm^3), for a long enough operation time in the constant pumping out regime ($t_1 - t_0 = 40$ min and $t_2 - t_0 = 80$ min), pressure in the measuring volume and intensities of the $^3T^+ - {}^3He^+$ and $^3T_2^+$ peaks decreased by approximately 10% of their initial value. After pressure recovery in the measuring volume at the instant $t_3 =$ 120 min, the intensities of the peaks also returned to their initial values.

The results of analysis of the gas mixture containing tritium obtained with the time-of-flight mass reflectron are presented in Table 2. We did not find the influence of the background current caused by the β decay of tritium nuclei on the intensity of measured peaks and errors in measuring gas components, although measurements were performed for more than two hours. It is known from previous experiments with tritium that the background current begins to increase at once after tritium admission into the analyzer. We can see from Table 2 that the unresolved $^3T^+ - {}^3He^+$ peak intensity considerably exceeds the intensity of the molecular tritium $^3T_2^+$ peak. It seems that this is explained by the fact that the age of the tritium sample exceeded 20 years and a considerable part of the tritium decomposed, transforming into helium-3, which we detected.

These experiments showed that the time-of-flight spectrometer operating in the synchronous detection regime allows us to exclude the influence of the background current of tritium β electrons and to analyze with high precision the composition of tritium-containing gas mixtures. The main advantage of mass reflectrons for analyzing fuel gas mixtures is their considerably higher resolving power [70, 71] than that of other instruments.

10. Enhanced resolving power mass reflectron

The main components of fuel gas mixtures for thermonuclear reactors are hydrogen isotopes: protium, deuterium, and tritium, and also two helium isotopes, ^3He and ^4He.

Figure 7 shows the calculated spectrum of such a mixture and the resolving powers required for the complete separation of two adjacent lines of the mass spectrum [7]. It can be seen from this figure that the complete separation of multiplets of single-charged ions requires a resolving power of mass spectrometers of $\approx 3 \times 10^3$, while to separate the $^3T^+ - {}^3He^+$ doublet, the resolving power based on the mass peak should be $R = 1.5 \times 10^5$. The required resolving power at the 10% level of the mass peak height and lower will be determined by the component content ratios in the gas mixture. Because component ratios can be $10^3 - 10^4$, a high isotopic sensitivity of the mass spectrometer is also required, which is mainly determined by the resolving power, the shape of lines in the mass spectrum, and the presence of 'tails' of the peaks. As mentioned above, the presence of small amounts of heavy impurities (N_2, O_2, Ar) in fuel gas mixtures at a level of $10^{-2} - 10^{-3}$% also requires a high absolute sensitivity of mass spectrometers.

The design of mass reflectrons satisfies these requirements, because they do not contain aperture slits and the cross section of an ion beam in the source, reflector, and detector, which is restricted only by the size of the input dynode of a secondary electron multiplier or the area of microchannel plates, can exceed 10 cm^2. The absence of the discrimination of ions by their mass in the source and the high transparency of grids in the source and reflector, which can reach 90%, also favors the achievement of high absolute and isotopic sensitivities of these instruments. A complete and reliable analysis of hydrogen–helium mixtures should take into account the presence of protium, deuterium, and tritium atoms in all molecules contained in these mixtures.

One can see from Fig. 7 that, to separate all trimer peaks (H_3^+, H_2D^+, HD_2^+, HDT^+), the resolving power $R \geqslant 3 \times 10^3$ is needed, which can hardly be achieved in the near future in mass reflectrons of the usual design and reasonable size without multiple reflections [72]. However, deuterium and tritium contained in trimers can be taken into account by

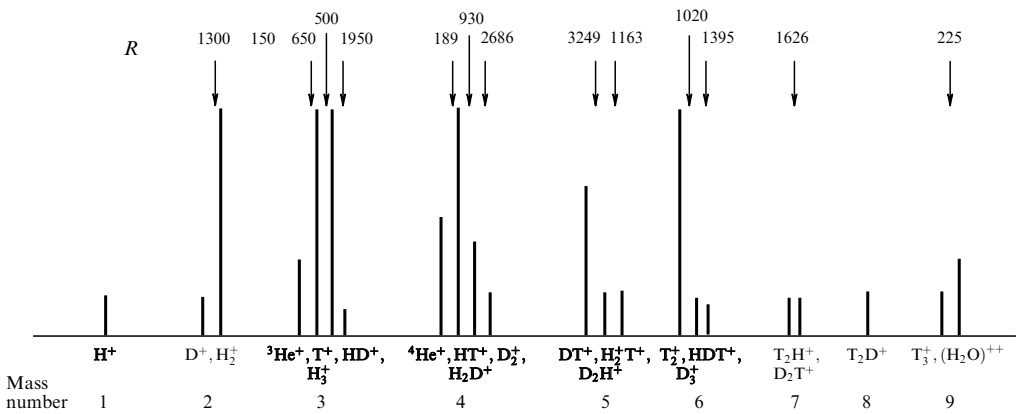

Figure 7. Calculated mass spectrum for a mixture of hydrogen and helium isotopes. At the top are indicated resolving powers R by peak bases required for resolving two adjacent lines.

calibrating the instrument with the help of standard mixtures by determining the ratios of atomic, molecular, associated, and trimer peaks of protium, deuterium, and tritium. It is known from the literature that the ratio of trimer and molecular mass lines for protium and deuterium lie in the range from 2×10^{-5} to 10^{-3} [30, 73, 74]. The ratios of atomic and molecular peaks in the mass spectra of gas mixtures containing hydrogen isotopes lie in the range from 0.01 to 0.03, depending on measurement conditions, in particular, on the energy of ionizing electrons, the degree of clearing and washing the mass analyzer, the presence of heating, pumping out, etc. [30, 74].

The intensity of associated HD^+, HT^+, and DT^+ peaks in mass spectra is determined by the concentration of isotopes in a gas mixture and depends on temperature and the mixing time. It is known that the rate of ion-exchange reactions at room temperature is small, and a change in the temperature in the electron gun region during a prolonged continuous operation of the analyzer, although weak, will affect the ratio of associated and molecular peaks. This means that the cathode filament current, electron emission current, and energy of ionizing electrons should be minimal to ensure the required operation regime of the instrument.

The main requirement for the resolving power of the mass reflectron for the given problem is the resolution of the multiplet with $M = 3$ a.m.u. The resolution of the $^3He^+ - {}^3T^+$ doublet has been reported many times, while to resolve the associated HD^+ peak and trimer H_3^+ peak, the resolving power of ≈ 1940 is needed. Therefore, the separation of two unresolved doublets $^3He^+ - {}^3T^+$ and $HD^+ - H_3^+$ is the necessary condition. This can be achieved if the resolving power of the instrument based on the mass line is no less than 500. The contribution of atomic tritium to the unresolved $^3He^+ - {}^3T^+$ peak can be estimated from the previously determined ratio of atomic and molecular tritium peaks. The contribution of the associated HD^+ peak and trimer H_3^+ peak can be estimated from calibration measurements with standard mixtures. For the resolving power of the instrument $R \sim 500$, the multiplet with $M = 4$ a.m.u. will consist of two peaks: the $^4He^+$ peak and the unresolved $HT^+ - D_2^+ - H_2D^+$ triplet peak. The relative contribution of the H_2D^+ trimer to the unresolved peak intensity probably will not exceed 10^{-3}, and the contribution of HT^+ will be no more than $\approx 10^{-2}$, taking into account that the content of protium in fuel mixtures should not exceed 1%. Thus, the main contribution to the unresolved $HT^+ - D_2^+ - H_2D^+$ peak belongs to molecular deuterium.

The estimates presented above are based on the fact that the amount of substance in components of the gas mixture is proportional to the intensity of peaks in the mass spectrum, in particular, unresolved peaks. Note that the more accurate method for determining substance amount ratios is based on the measurement of the mass peak area, rather than its amplitude. In the case of unresolved peaks, their broadening and increase in area allow us to take into account small amounts of substance. The mass spectrometer is calibrated by all components of the mixture, and all coefficients relating the amount of substance to the mass peak area are determined during calibration. For this purpose, standard gas mixtures with an accurately known composition are used. In [70], the compositions of three standard mixtures with different contents of the required components are proposed for calibration of mass reflectrons used to analyze fuel hydrogen–helium mixtures.

As mentioned above, the resolving power of time-of-flight mass spectrometers (20) is proportional to the time of flight T of ions from the source to detector and is inversely proportional to the duration Δt of ion packets in the entrance plane to the detector.

Consider in more detail the factors reducing the resolving power of time-of-flight electron ionization mass spectrometers. Because the time of flight T is proportional to the square root of the ion mass M and Δt depends on all aberrations of the instrument and cannot be shorter than the response time of the detector to the arrival of one ion, which is virtually independent of the ion mass, R decreases with decreasing ion mass.

We calculated a mass reflectron with the required resolving power of about 500 or more by the mass spectrum peak base for $M = 3$ a.m.u. taking into account that different types of ion sources exist: single-gap, two-gap, and three-gap. The sources of all types have the common property that light ions, which have higher velocities at a certain temperature, manage to occupy a greater volume $V = \Delta x \Delta y \Delta z$ of the ionization gap during ionization than heavy ions. Therefore, the initial width Δx of the packet of light ions is greater than that of heavy ions, which causes the broadening of mass spectrum lines in the region of light ion masses. In addition, the increase in ΔU leads to an increase in the initial energy spread ΔU of light ions compared to that of heavy ions. When ions are turned by the front of the ejecting pulse, light ions receive the additional energy spread ΔU at the source exit, which also causes additional broadening of the mass peak. Both factors (the increase in Δx and ΔU) reduce the resolving power in the region of light ion masses compared to that in the region of heavy ion masses. Obviously, the aim of the source calculation is the simultaneous reduction in the spatial Δx and energy ΔU ion spreads. By introducing the energy spread coefficient for ions in the source defined as $k = U_{\max}/U_{\min}$ (where $U_{\max}$ and $U_{\min}$ are the maximum and minimum ion energies), we obtain for the two-gap source the typical energy spread with $k \approx 1.2$. The numerical simulation and calculations performed made it possible to determine geometrical parameters and to choose a two-gap source with $k \approx 1.18$ and $\Delta x \approx 0.7$ mm as the optimal variant.

In [70], a method for calculating the parameters of a two-gap reflector was proposed which provides the optimal focusing of ions with the specified energy ratio $k = U_{\max}/U_{\min}$. Unlike conditions for the reflector in [59], the focusing conditions do not require the coincidence of the roots of the first and second derivatives, but these roots should only lie in the interval between $U_{\min}$ and $U_{\max}$. This allows selecting the reflector parameters so that the resolving power by the compensation factor of the ion energy spread increases twofold. We calculated the reflector by using the expression for the time of flight of a single ion with the charge q and mass M through the reflector [see Eqn (19)], which can be represented by the function f depending only on dimensionless parameters,

$$L_{\mathrm{dr}} \left(\frac{M}{2qU_T} \right)^{1/2} = f(k, \lambda, \mu, \nu, y) \,, \tag{31}$$

where L_{dr} is the drift gap, U_T is the potential across the braking grid, $k = U_{\max}/U_{\min}$ is the energy spread of ions in the source, $\lambda = d_T/L_{\mathrm{dr}}$, d_T is the braking gap of the reflector, $\mu = d_{\mathrm{ref}}/L_{\mathrm{dr}}$, d_{ref} is the reflecting gap of the reflector, $\nu = U_{\mathrm{ref}}/U_T$, $U_{\mathrm{ref}}(U_{\max})$ is the potential across the reflecting grid, and $y \equiv U/U_T$, U is the potential energy of a probe ion.

The reflector is calculated by constructing and minimizing the dimensionless functional

$$(\Delta t)^2 = \frac{1}{y_{\max} - y_{\min}} \int_{y_{\min}}^{y_{\max}} \mathrm{d}y (f - f_{\mathrm{mid}})^2 , \qquad (32)$$

where

$$f_{\mathrm{mid}} = \frac{1}{y_{\max} - y_{\min}} \int_{y_{\min}}^{y_{\max}} \mathrm{d}y f ,$$

$y_{\max} = U_{\max}/U_T$ and $y_{\min} = U_{\min}/U_T$. It follows from (32) that the values of functional $(\Delta t)^2$ depend only on dimensionless coefficients k, λ, μ, and ν and, therefore, the value of L_{dr} can be chosen independently of the reflector parameters. After the choice of L_{dr}, the values of d_T and d_{ref} are calculated. In this case, each calculated reflector will be optimal for compensating the fixed energy spread k. It turns out that there are no restrictions on the choice of the braking gap d_T, and it can be chosen arbitrarily as the parameter λ containing d_T.

The third element determining the operation of the TFMS mass reflectron is a detector. To optimize the detector operation in the enhanced resolving power instrument, the ratio V/l was increased, where V is the voltage between the output microchannel plate and the electron collector and l is the distance between them. This reduced the aberration $\Delta T_{\Delta t}$ related to microchannel plate response time Δt per ion. Measurements showed that Δt decreased by several times and did not exceed 1 ns.

After the brief discussion of operation of the main elements of the mass reflectron, we consider the influence of aberrations on the resolving power of the instrument as a whole. Equation (20) for the resolving power of a time-of-flight instrument with the reflector at the mass peak half-maximum can be written in the form [71]

$$R = \frac{T}{\sum_i \Delta T_i} = \frac{T}{\sum_i \Delta T_i + \left[\sum_j (\Delta T_j)^2\right]^{1/2}} = \frac{1}{\sum_i 1/R_i + \left[\sum_i (1/R_i)^2\right]^{1/2}} , \qquad (33)$$

where T is the total time of flight from the source to detector and $1/R_i = \Delta T_i/T$. It follows from (33) that the resolving power R of the mass reflectron depends on the resolving power R_i over the ith aberration factor in a complicated way. Each R_i depends on many physical parameters of the instrument and, therefore, it is impossible to use expression (33) for the optimization of analytic characteristics of the mass spectrometer.

The problem of obtaining the maximum resolving power of the mass reflectron was solved as follows. Based on our experimental data, we constructed a hierarchy of resolving powers $R_1 \leqslant R_2 \leqslant R_3 \leqslant \ldots \leqslant R_k$ and then performed calculations. Because the influence of R_1 on the total resolving power R is dominating, the physical parameters of the problem are changed so as to provide an increase in R_1. Similar operations were performed with R_2, R_3, etc. In this case, the principle should be fulfilled according to which calculations resulted in the increase in the lowest resolving power R_i. Our experience shows that R_i seldom combine in groups of two or more aberration factors with close resolving powers.

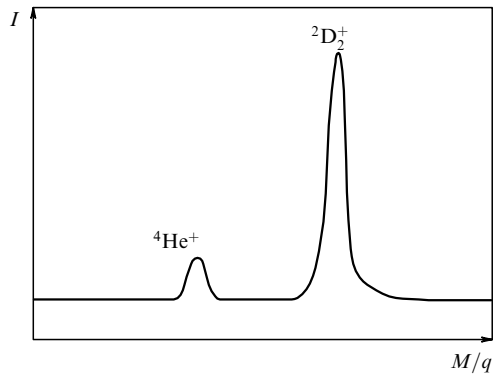

Figure 8. Mass spectrum of a gas $^4He^+ - {}^2D_2^+$ mixture containing $\approx 15\%$ helium. $\Delta M = 0.0256$ a.m.u.

The second principle of using expression (33) in the calculation of the TFMS is based on the division of the ion trajectory into two regions: from the source to the first focus located between the source and reflector, and from the first focus to the second focus located in the detector plane. The second region contains the reflector. The problem is solved from the end. First the reflector and initial conditions for the phase volume in the first focus are calculated, and then the source parameters creating the phase volume elements Δx, ΔU in the focus of the source are selected.

Based on these calculations, the mass reflectron was developed and constructed with the analyzed chamber 80 cm in length and the ion drift length about 90 cm in length [71]. The results of calculations of geometrical and electric parameters and analytic characteristics of the instrument were completely confirmed in experiments.

Figure 8 shows the mass spectrum of the $^4He + {}^2D_2$ gas mixture containing about 15 volume percent of helium recorded for the first time with a time-of-flight mass reflectron. The mass spectrum demonstrates that the resolving power of the instrument at the 10% level of the peak amplitude is ≈ 600. As mentioned above, this resolving power provides the reliable resolution of two unresolved doublets $^3He^+ - {}^3T^+$ and $HD^+ - H_3^+$ at the mass number 3 a.m.u. and the separation of the $^4He^+$ peak from the unresolved $HT^+ - D_2^+ - H_2D^+$ triplet at the mass number 4 a.m.u. Thus, the developed mass reflectron allows us to solve to a considerable extent the problem of quite accurate continuous chemical and isotope analysis of hydrogen–helium tritium-containing gas mixtures, which is very important for further studies in the field of controlled thermonuclear fusion, including the ITER.

11. Conclusion

Two types of dynamic mass spectrometer, magnetic resonance mass spectrometers and time-of-flight mass spectrometers called mass reflectrons, developed at the laboratory of mass spectrometry at the Ioffe Institute, RAS have high analytic characteristics and can operate in different regimes. The field of applications of these instruments in science and technology is broad and diverse: from the study of individual events in nuclear reactions or decoding of the genomes of living creatures to the control of rapid pyroprocesses in melting a few dozen tons steel at metallurgic plants.

Time-of-flight mass reflectrons are produced in great numbers by many instrument making companies all over the

world. They are in high demand, simple to manufacture and operate, and relatively low in cost. Magnetic resonance mass spectrometers are purely Russian instruments, and only seven such spectrometers have been built. These are intricate and costly instruments with unique analytic characteristics. Suffice it to say that they allow us, for example, to measure simultaneously with a high accuracy two helium isotopes in a gas mixture where the amount of heavy ^{4}He isotope can be 10^{10} times greater than that of the light ^{3}He isotope. Due to their very high analytic characteristics, these instruments are always in demand by researchers in geology, geochronology, space chemistry, solid state physics, nanomaterials, plasma physics, nuclear technologies, etc. Unfortunately, these instruments were built about 40 years ago, and at present considerable investments are required for their repair, their updating, and increasing the operation reliability.

References

1. Tret'yakov E F et al. *Bull. Acad. Sci. USSR Phys. Ser.* **40** (10) 1 (1976); *Izv. Akad. Nauk SSSR Ser. Fiz.* **40** 2026 (1976)
2. Lyubimov V A et al. *Sov. Phys. JETP* **54** 616 (1981); *Zh. Eksp. Teor. Fiz.* **81** 1158 (1981)
3. Simpson J J *Phys. Rev. D* **23** 649 (1981)
4. Nikolaev E N et al. *JETP Lett.* **39** 534 (1984); *Pis'ma Zh. Eksp. Teor. Fiz.* **39** 441 (1984)
5. Lippmaa É T et al. *JETP Lett.* **39** 646 (1984); *Pis'ma Zh. Eksp. Teor. Fiz.* **39** 529 (1984)
6. Chastagner P, Daves H L, Hess W B *Int. J. Mass Spectrom. Ion Phys.* **48** 353 (1983)
7. Alekseenko S A et al. *Sov. Atom. Energy* **51** 436 (1981); *Atom. Energ.* **51** (1) 27 (1981)
8. Ferguson R B, Chastagner P *Int. J. Mass Spectrom. Ion Phys.* **24** 403 (1977)
9. Maroni V A, Van Deventer E N *J. Nucl. Mater.* **85–86** 257 (1979)
10. Unterweger M P et al. *Int. J. Appl. Radiat. Isot.* **31** 611 (1980)
11. Mamyrin B A, Aruev N N, Alekseenko S A *Sov. Phys. JETP* **36** 1 (1973); *Zh. Eksp. Teor. Fiz.* **63** 3 (1972)
12. Bleakney W, Hipple J A (Jr.) *Phys. Rev.* **53** 521 (1938)
13. Goudsmit S A *Phys. Rev.* **74** 622 (1948)
14. Fiks V B, in *Doklady Nauchno-Tekhnicheskoi Konf. LPI* (Proc. of the Scientific and Technical Conf., LPI) (Leningrad: LPI, 1949) p. 25
15. Smith L G *Rev. Sci. Instrum.* **25** 115 (1951)
16. Ionov N I, Mamyrin B A, Fiks V B *Zh. Tekh. Fiz.* **23** 2104 (1953)
17. Mamyrin B A, Shustrov B N *Zh. Tekh. Fiz.* **27** 1347 (1957)
18. Shustrov B N *Sov. Phys. Tech. Phys.* **5** 810 (1961); *Zh. Tekh. Fiz.* **30** 860 (1960)
19. Bennett W H *J. Appl. Phys.* **21** 143 (1950)
20. Mamyrin B A, Frantsuzov A A *Prib. Tekh. Eksp.* (3) 114 (1962)
21. Mamyrin B A, Shustrov B N *Prib. Tekh. Eksp.* (5) 135 (1962)
22. Mamyrin B A, Frantsuzov A A, in *Atomic Masses. Proc. of the Third Intern. Conf., 28 August – 1 September, 1967, Winnipeg, Canada* (Ed. R C Barber) (Winnipeg: Univ. of Manitoba Press, 1967) p. 427
23. Mamyrin B A, Frantsuzov A A *Sov. Phys. JETP* **21** 274 (1965); *Zh. Eksp. Teor. Fiz.* **48** 416 (1965)
24. Mamyrin B A, Aruev N N, Alekseenko S A, Author's Certificate No. 445901; *Byull. Izobret.* (37) 113 (1975)
25. Alekseenko S A, Aruev N N, Mamyrin B A *Metrologiya* (4) 54 (1974)
26. Cohen E R, Taylor B N *J. Phys. Chem. Ref. Data* **2** 663 (1973)
27. Cohen E R, Taylor B N *Rev. Mod. Phys.* **59** 1121 (1987)
28. Mamyrin B A, Alekseenko S A, Aruev N N *Sov. Phys. JETP* **53** 1109 (1981); *Zh. Eksp. Teor. Fiz.* **80** 2125 (1981)
29. Malinowski M E, SAND 79-8218 (Livermore: Sandia Laboratories, 1979)
30. Ellefson R E, Moddeman W E, Dylla H F *J. Vac. Sci. Technol.* **18** 1062 (1981)
31. Aruev N N, Baidakov E L, Mamyrin B A, Alekseenko S A, Author's Certificate No. 1123392; *Byull. Izobret.* (11) (1986)
32. Aruev N N, Baidakov E L, Mamyrin B A *Sov. Phys. Tech. Phys.* **32** 180 (1987); *Zh. Tekh. Fiz.* **57** 300 (1987)
33. Kuprevich V V, Lunter S G *Opt.-Mekh. Prom.* (9) 51 (1969)
34. Jones P M S *J. Nucl. Mater.* **21** 239 (1967)
35. Rudy C R, Jordan K C, Mound Laboratory Report MLM 2458 (Miamisburg, Ohio: Monsanto Res. Corp., 1977)
36. Jordan K C, Blanke B C, Dudley W A *J. Inorg. Nucl. Chem.* **29** 2129 (1967)
37. Shimanskaya N S, Preprint RI-111 (Leningrad: Khlopin Radium Institute, 1979)
38. Tikhonov V N, Chukreev F E, Preprint IAE-3102 (Moscow: Kurchatov Atomic Energy Institute, 1979)
39. Akulov Yu A et al., Author's Certificate No. 1295918; *Byull. Izobret.* (4) 265 (1988)
40. Mamyrin B A et al. *Prib. Tekh. Eksp.* (2) 151 (1982)
41. Mamyrin B A et al. *Zh. Tekh. Fiz.* **53** 1139 (1983)
42. Anufriev G S et al. *Prib. Tekh. Eksp.* (4) 211 (1979)
43. Akulov Yu A et al. *Sov. Tech. Phys. Lett.* **14** 416 (1988); *Pis'ma Zh. Tekh. Fiz.* **14** 940 (1988)
44. Akulov Yu A, Mamyrin B A *Phys. Usp.* **46** 1153 (2003); *Usp. Fiz. Nauk* **173** 1187 (2003); Mamyrin B A, Akulov Yu A *Phys. Usp.* **47** 729 (2004); *Usp. Fiz. Nauk* **174** 791 (2004)
45. Gusev V K et al. *Tech. Phys.* **44** 1054 (1999); *Zh. Tekh. Eksp.* **69** (9) 58 (1999)
46. Aruev N N, Boltenkov B S, Novokhatsky A N *Int. J. Mass Spectrom.* **351** 76 (2013)
47. Akulov Yu A et al. *Prib. Tekh. Eksp.* (2) 173 (1985)
48. Mamyrin B A, Tolstikhin I N *Helium Isotopes in Nature* (Amsterdam: Elsevier, 1984)
49. Aruev N N, Boltenkov B S *Tech. Phys. Lett.* **36** 337 (2010); *Pis'ma Zh. Tekh. Fiz.* **36** (7) 89 (2010)
50. Anufriev G S et al. *Prib. Tekh. Eksp.* (1) 248 (1977)
51. Alekseichuk B K et al. *Prib. Tekh. Eksp.* (4) 206 (1979)
52. Cameron A E, Eggers D F (Jr.) *Rev. Sci. Instrum.* **19** 605 (1948)
53. Ionov N I, Mamyrin B A *Zh. Tekh. Fiz.* **23** 2101 (1953)
54. Wiley W C, McLaren I H *Rev. Sci. Instrum.* **26** 1150 (1955)
55. Agishev E I, Ionov N I *Zh. Tekh. Fiz.* **26** 203 (1956)
56. Agishev E I, Ionov N I *Zh. Tekh. Fiz.* **28** 1776 (1958)
57. Alikhanov S G *Sov. Phys. JETP* **4** 452 (1957); *Zh. Eksp. Teor. Fiz.* **31** 517 (1956)
58. Mamyrin B A, Author's Certificate No. 198034 (1966); *Byull. Izobret.* (13) 148 (1967)
59. Karataev V I, Mamyrin B A, Shmikk D V *Sov. Phys. Tech. Phys.* **16** 1177 (1972); *Zh. Tekh. Fiz.* **26** 1498 (1971)
60. Mamyrin B A et al. *Sov. Phys. JETP* **37** 45 (1973); *Zh. Eksp. Teor. Fiz.* **64** (1) 82 (1973)
61. Shmikk D B, Dubenskii B M *Zh. Tekh. Fiz.* **54** 912 (1984)
62. Karataev V I, Aruev N N *Tech. Phys. Lett.* **37** 575 (2011); *Pis'ma Zh. Tekh. Fiz.* **37** (12) 67 (2011)
63. Karataev V I *Tech. Phys. Lett.* **19** 498 (1993); *Pis'ma Zh. Tekh. Fiz.* **19** (15) 65 (1993)
64. Karataev V I *Tech. Phys. Lett.* **24** 167 (1998); *Pis'ma Zh. Tekh. Fiz.* **24** (3) 1 (1998)
65. Karataev V I *Tech. Phys. Lett.* **34** 1082 (2008); *Pis'ma Zh. Tekh. Fiz.* **34** (24) 90 (2008)
66. Shmikk D V *Sov. Phys. Tech. Phys.* **26** 615 (1981); *Zh. Tekh. Fiz.* **51** 1024 (1981)
67. Tuchkevich V M *Vestn. Akad. Nauk SSSR* (5) 59 (1985)
68. Mamyrin B A et al. *Tech. Phys.* **38** 1033 (1993); *Zh. Tekh. Fiz.* **63** (11) 200 (1993)
69. Aruev N N et al. *Tech. Phys. Lett.* **23** 811 (1997); *Pis'ma Zh. Tekh. Fiz.* **23** (20) 83 (1997)
70. Aruev N N et al. *Atom. Energy* **104** 308 (2008); *Atom. Energ.* **104** (4) 233 (2008)
71. Aruev N N, Zhdan V T, Kozlovskii A V *Mass-Spektrometrom.* **5** (4) 289 (2008)
72. Verentchikov A N et al. *Tech. Phys.* **50** 73 (2005); *Zh. Tekh. Fiz.* **75** (1) 74 (2005)
73. von Seggern J et al. *J. Vac. Sci. Technol. A* **2** 1516 (1984)
74. Engelmann U et al. *Nucl. Instrum. Meth. Phys. Res. A* **302** 345 (1991)